ELSEVIER

Journal of Atmospheric and Solar-Terrestrial Physics 68 (2006) 134–162

Journal of ATMOSPHERIC AND SOLAR-TERRESTRIAL PHYSICS

www.elsevier.com/locate/jastp

Topside ionospheric scale height analysis and modelling based on radio occultation measurements

S.M. Stankov*, N. Jakowski

German Aerospace Centre (DLR), Institute of Communications and Navigation (IKN), Department of Navigation and Guidance Systems, Kalkhorstweg 53, D-17235 Neustrelitz, Germany

Received 3 December 2003; received in revised form 11 April 2005; accepted 6 October 2005

Abstract

The knowledge of the scale height in the topside ionosphere region remains rather poor due to the insufficient observations carried so far. To advance this knowledge, presented here is a new method of retrieving the topside ionospheric scale height based on radio occultation observations onboard low-earth-orbiting satellites. The scale height, well known for its dependence on the temperatures and masses of the ionospheric constituents, understandably experiences large spatial and temporal variability. With the help of the CHAMP satellite's occultation experiment, analysed is the scale height behaviour with respect to solar and geomagnetic activity, local time, season, longitude and latitude. The expected strong dependence on temperature has been confirmed; however, it has been found that this dependence is not straightforward but more complex and clearly affected by other factors. For example, while the daytime scale height values increase at higher solar activity, the night-time values do not show such a trend. The seasonal dependence proved to be strong with summer-time values significantly higher than winter-time numbers. Also, there is no common pattern for the diurnal variations: sometimes daytime values are higher, sometimes the night-time values dominate; large differences are detected from season to season and from latitude to latitude. Generally, the scale increases at higher latitudes, although a few differences do exist. No major longitudinal and hemispheric differences have been detected so far. Based on the accumulated data, a first attempt has been made to empirically simulate the scale height value at 425 km altitude; as input parameters, the model respects the local time, latitude, and season. The scale height model can be implemented into the electron density profile retrieval procedure by delivering an improved initial guess.

Keywords: Ionosphere; Radio occultation; Scale height; Empirical modelling

1. Introduction

One of the most important characteristics of the ionosphere–plasmasphere system is the plasma scale height. The plasma scale height has the dimension of length and is defined (Davies, 1990; Hargreaves, 1992) as $H_P = kT_P/m_i g$, where m_i is the ion mass, $T_P = T_i + T_e$ is the plasma temperature, T_i and T_e—ion and electron temperatures, k—the Boltzmann constant (1.380658×10^{-23} J/deg). Actually, the scale height is a critical property of any atmosphere and can be defined for each ion or neutral constituent (Van Zandt, 1967). In practice, the vertical scale height can be approximately deduced

*Corresponding author. Tel.: +49 3981 480 113; fax: +49 3981 480 123.

E-mail address: stanimir.stankov@dlr.de (S.M. Stankov).

1364-6826/$ - see front matter © 2005 Elsevier Ltd. All rights reserved.
doi:10.1016/j.jastp.2005.10.003

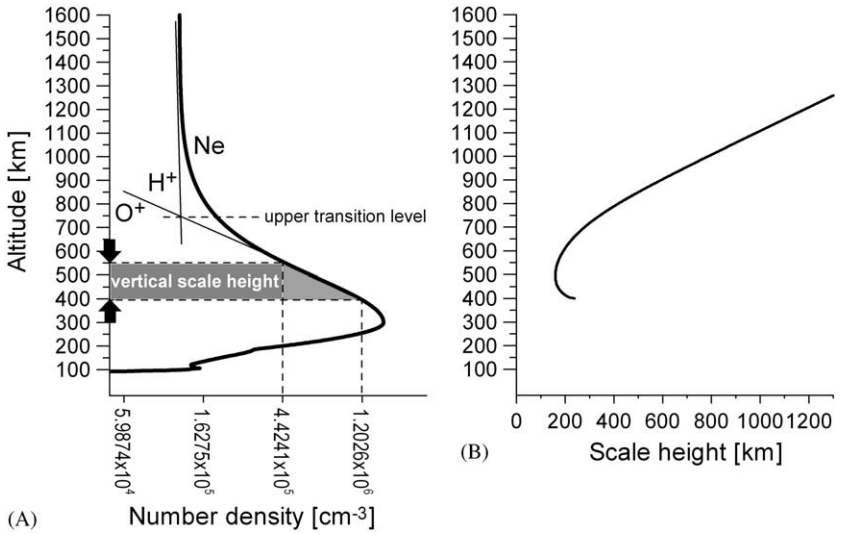

Fig. 1. Schematic view of the O^+, H^+, and Ne vertical profiles (Panel A) and the derivation of the vertical plasma scale height. Notice the altitudinal variation of the topside plasma scale height (Panel B).

(Fig. 1A) as the vertical distance in which the concentration changes by a factor of an exponent ($e \approx 2.718281828$). Since the plasma temperature varies with altitude, it is obvious that the plasma scale height varies as well (Fig. 1B). Also, the value of the plasma scale height indicates the gradient of the electron density; for instance, in the topside ionosphere region—the region situated immediately above the height (h_mF_2) of the ionospheric F2 peak electron density—the steeper the electron density profile, the larger is the scale height. Because many ionospheric phenomena leave their signatures on the scale height, a study of the scale height behaviour can provide valuable information on the vertical distribution of ionisation, and can thus be capable of answering many open questions in the ionospheric physics, particularly those related to ionosphere composition and dynamics (Hanson and Ortenburger, 1961; Horwitz et al., 1990; Rawer, 1993). The knowledge of the scale height value is of particular importance in several scientific and technical applications. For many years, simple ionospheric profilers, such as the Exponential, Chapman, and Epstein layers (Banks and Kockarts, 1973; Rawer, 1988; Stankov, 2002b), have been used to model the topside ionosphere, e.g. in the International Reference Ionosphere (IRI) empirical model (Bilitza, 2001). Also, in the software for inversion of ionograms in modern digital ionosondes, the Epstein formulae are applied to complement the deduced bottom-side electron profile with a topside profile (Reinisch, 1996; Reinisch and Huang, 2001). However, because the topside scale height is unknown, it is assumed that the scale height above the F2 peak equals the scale height just below the peak; this is a strong assumption which is not always correct. There are also density reconstruction techniques which could significantly benefit from the knowledge of the topside ionospheric scale height, at least as a source of an educated initial guess (Jakowski et al., 2002b; Heise et al., 2002; Stankov et al., 2003a).

The bottom-side scale height is relatively well known and easy to deduce thanks to the ground ionosonde measurements and the dense network of such ionosondes. The scale height in the plasmasphere is also relatively easy to calculate because it is changing slowly with altitude (due to the small gradient in the plasma temperature) and increasing number of in-situ measurements (both on plasma density and temperature). The plasma scale height in the topside ionosphere—from h_mF_2 up to the O^+–H^+ ion transition level, where the plasmasphere starts, is most difficult to obtain. The abundant ground ionosonde measurements are not helpful at all because they sound the bottom-side ionosphere up to h_mF_2. Besides, the temperature changes in the topside ionosphere are large and vary widely with local time (LT), season and latitudes which lead to large variations in the scale height too.

There are several techniques which have been used for gathering information on the topside

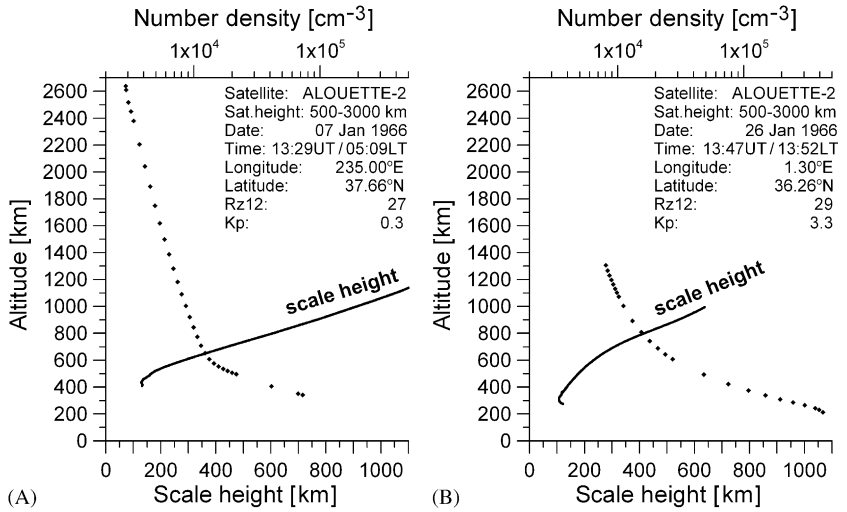

Fig. 2. The plasma scale height (solid line) deduced from topside sounding measurements onboard Alouette-2. The electron density values (dots) obtained from manually scaled ionograms and using the inversion algorithm of Jackson (1969).

ionosphere and which can also be used for scale height investigation, most prominent of them being the in-situ measurements (Pfaff, 1996), incoherent scatter radar (ISR) probing, and topside sounding (TS) onboard satellites. The ISR probing (Gordon, 1958; Bowles, 1958; Beynon and Williams, 1978; Farley, 1996) is a powerful technique capable of simultaneously measuring range-resolved ionospheric and atmospheric parameters, including ionospheric temperatures and scale heights (Van Zandt and Bowles, 1960), from the ground, through the topside ionosphere, up to very high altitudes. Also, it is possible with this technique to obtain spatial coverage in both latitude and longitude. Several facilities around the globe are currently in operation: EISCAT, Svalbard, Sondrestrom, Millstone Hill, Arecibo, Jicamarca, etc. Although providing high-quality measurements, these facilities are complex and expensive installations that need a lot of resources to be maintained. The topside sounders (Franklin and Maclean, 1969) are constructed similar to the ground ionosonde. However, placed onboard satellites (typically at 1000–1500 km altitude), they sound the ionosphere from above. There were several satellites carrying topside sounders, such as the Alouette and ISIS satellite series, but the coverage has not been continuous. Still, the technique provides good geographic coverage although at the expense of LT coverage. Also, the ionogram inversion (Jackson, 1969) is a bit complicated due to the existence of additional signals, the resonance spikes. However, it is relatively easy to deduce the plasma scale height from the TS data (Fig. 2).

Here, we present another way of studying the topside scale height—the Ionospheric Radio Occultation (IRO) observations performed with the help of the Global Navigation Satellite Systems (GNSS) and Low Earth Orbiting (LEO) satellites. It provides excellent opportunities for observation of the topside ionosphere parameters on a global scale (Jakowski et al., 2002b, 2005a). The purpose of this publication is to present the experience in retrieving, analysing, and simulating the topside ionospheric scale height based on the IRO measurements onboard the German LEO satellite CHAMP (CHAllenging Minisatellite Payload) (Reigber et al., 2003). Here, the scale height value is obtained directly from the vertical electron density profile retrieved by IRO measurements. Latitudinal and seasonal variations of the plasma scale height have been obtained for both day- and night-time conditions. Based on the accumulated database, a first version of an empirical model has already been developed (Stankov and Jakowski, 2005). Considering the increased knowledge of the scale height behaviour, the steady growing CHAMP measurement database, and the increasing number of LEO satellites, it will be possible to further develop the model. The latter can be used in various scientific and technical applications—investigating the ionosphere–plasmasphere composition and dynamics, improving the IRO profile retrieval, developing novel reconstruction techniques (Stankov et al.,

2003a, 2005), operational monitoring of the ionosphere density distribution (Stankov et al., 2003b), etc.

This publication is structured as follows. First, the IRO measurement technique is outlined. Second, the topside scale height retrieval is described. Next, the database is detailed. Then, the scale height behaviour is investigated, including dependencies on solar and geomagnetic activity, local time, season, latitude and longitude. Finally, the first results in the empirical modelling of the topside scale height are provided. The main outcomes and possible applications are summarised in the last section.

2. The method

The GNSS-based radio occultation measurements establish the foundation of a novel remote sensing technique capable of reliably deducing the electron density distribution in the entire ionosphere from the GNSS satellite heights down to the bottom ionosphere heights.

2.1. GPS radio occultation measurements of the ionosphere

Since a large number of ionospheric phenomena are accompanied by (or are due to) strong spatial plasma density gradients (particularly during ionospheric storms and/or near the crest region), and furthermore, because the path through the ionosphere is of length in the order of 1000–2000 km, the assumed spherical symmetry of the widely used Abel inversion technique does not, in general, hold. To overcome this methodological restriction, the following tomographic approach is adopted (Jakowski et al., 2002b). Considering the GPS signal frequencies L1 and L2, the ionospheric phase delay d_I may be estimated in a first-order approximation by

$$d_I = \frac{K}{f^2} \int n_e \, ds, \tag{1}$$

where $K = 40.3\,m^3/s^{-2}$, f is the signal frequency, and n_e is the electron density along the ray path s. Due to frequency dispersion, the difference between the L1 and L2 phases can be used to remove all other variable ranging parameters; thus, the differential GPS phases provide the total electron content (TEC) along the ray path through a spherically layered voxel structure. The dual frequency carrier phases of the GPS signals are used to compute the TEC along the 1 Hz sampled occultation ray paths. The measured line integral (TEC) is the sum of the product $n_e \times ds_i$ where n_e is the mean electron density in voxel i and ds_i corresponds to the ray path length in voxel i at measurement j. Simulations have shown that the ray path bending can be ignored in a first-order approximation; hence, the ray path elements can be computed easily according to the satellite geometry defined by the positions of the transmitting GPS satellite and the LEO satellite where the signal is received. An occultation event is defined by a series of TEC measurements along ray paths traversing the ionosphere with tangential heights of these ray paths decreasing to the bottom of the ionosphere (Fig. 3). The electron density in different shells can successively be derived from a series of 1 s sampled measurements j when the tangential point of occultation rays comes closer and closer to the Earth down to the bottom of the ionosphere. Constructed is a system of linear equations for the electron density in the different shells. If the electron density distribution above the top shell (traversed by the first ray of the occultation event) is available a priori (first guess), e.g. from a model, then the electron density in this top shell can be deduced. Hence, starting from the top shell, the electron density in each shell below can be successively determined. Finally, the solution of the above-mentioned system provides the IRO-based vertical electron density profile. The described tomographic approach has the advantage that additional information (e.g. horizontal gradients) from ground-based GPS measurements, models and/or other sources can easily be included in the reconstruction of the electron density profile, at least in the post-processing phase.

2.2. The CHAMP satellite mission

The German CHAMP satellite was successfully launched on 15 July 2000 into a near polar orbit, with an inclination of 87° and an initial altitude of 450 km. CHAMP orbits the Earth every 90 min shifting longitude by 11.75° west every orbit. Thus, an almost complete global coverage occurs every 24 h. The satellite is equipped with a dual frequency "Black Jack" GPS receiver which enables not only the analysis of the 0.1 Hz sampled navigation data (precise time and orbit information) but GPS radio occultation measurements as well. The receiver measures GPS carrier phases in the radio occultation or limb sounding mode starting at CHAMP

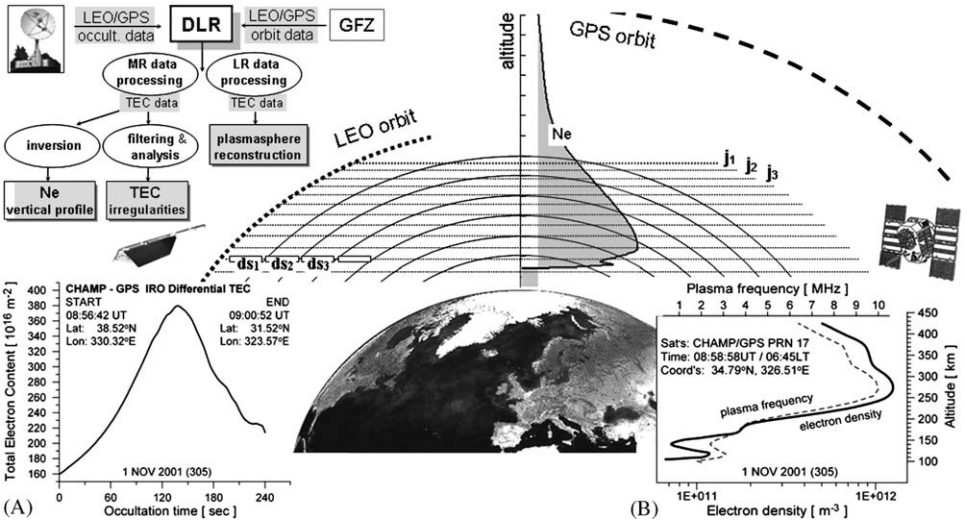

Fig. 3. Schematic view of the IRO retrieval procedure: CHAMP-GPS IRO differential TEC profile (Panel A) and the corresponding altitude profiles (Panel B) of the plasma frequency (dashed line) and the electron density (solid line). Low rate (0.1 Hz) data are used for plasmasphere reconstruction, while medium-rate (1.0 Hz) data are used for electron density profiling below the CHAMP orbit height.

orbit tangential heights down to the Earth surface with a sampling rate of 1 Hz. The CHAMP observations are first received at the DLR Remote Sensing Data Centre Neustrelitz and are then forwarded to the GeoForschungsZentrum (GFZ) in Potsdam. The measured GPS data are automatically checked and pre-processed by a highly flexible operational processing system (Wehrenpfennig et al., 2001). The processing flexibility is achieved thanks to the modular structure of the processing system in which the retrieval modules can be replaced and upgraded in the course of the CHAMP mission. The IRO measurements, carried out onboard CHAMP, started on 11 April 2001. By the end of June 2004, more than 180,000 occultations were recorded out of which more than 120,000 electron profiles were obtained.

2.3. Validation of CHAMP IRO measurements

Before practically using IRO retrieved electron density profiles their accuracy had to be evaluated under different geophysical conditions and with independent observations. The quality of the CHAMP IRO retrieval technique has been extensively validated using measurements from other techniques—in-situ probing (Jakowski et al., 2002b), ISR (Stolle et al., 2004), and vertical sounding (Jakowski et al., 2004, 2005b). Although, due to operational requirements, spherical symmetry of the ionospheric layers was assumed, the validation results are rather promising. A first opportunity to evaluate the accuracy of the IRO technique was the comparison with direct electron densities measured by the planar Langmuir probe onboard CHAMP. The comparison of the in-situ densities with the upper start values of the electron profiles showed quite a consistent correlation (Jakowski et al., 2002b). IRO-retrieved electron density profiles have been compared with vertical sounding measurements from several European digital ionosonde stations, such as Juliusruh (54.6°N; 13.4°E), Athens (38.0°N; 23.5°E), Rome (41.9°N; 12.5°E), Tortosa (40.8°N; 0.5°E) and Dourbes (50.1°N; 4.6°E). For example, a comparison made with data from the Juliusruh station during the first year of CHAMP IRO measurements yielded quite good results, particularly in the vicinity of the F2 peak density (Fig. 4). Additional comparison, between measurements of N_mF_2 and h_mF_2 deduced from IRO-based profiles and measurements from globally distributed ground ionosondes, resulted in standard deviations of 18% and 13%, respectively (Jakowski et al., 2004). A follow-on study, involving the above-mentioned European stations and data from the second year of the CHAMP IRO occultations, indicated a positive bias of the IRO data in the order of 0.5 MHz and a standard deviation from the mean of about 1 MHz (Jakowski et al., 2005b). Comparisons were also made between CHAMP IRO and EISCAT (European Incoherent Scatter) vertical electron density

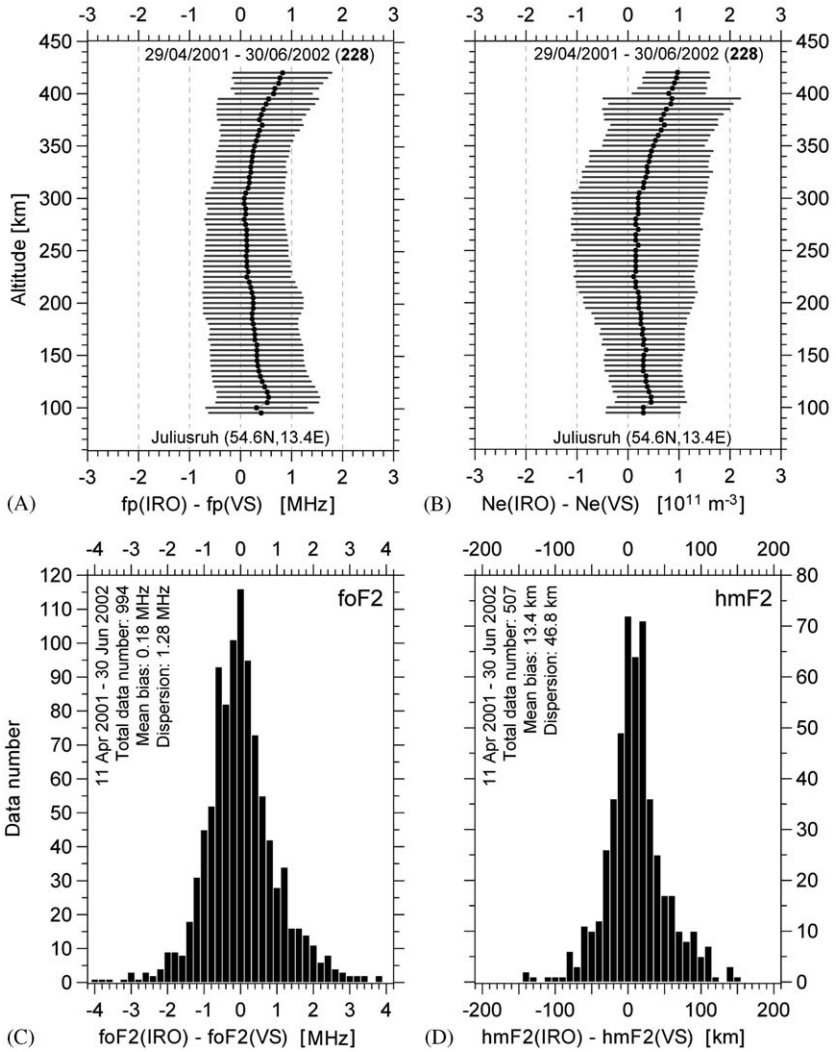

Fig. 4. Statistical comparison between the IRO and VS measurement techniques. Top panels: comparison between plasma frequency, f_p(IRO)–f_p(VS), and electron density, N_e(IRO)–N_e (VS) measurements at Juliusruh (54.6°N, 13.4°E); 228 profiles retrieved from 29/04/2001 to 30/06/2002, spatial coincidence radius of 6° and time difference of maximum 15 min. Bottom panels: comparison between critical frequency, foF_2(IRO)–foF_2(VS) and peak density height, h_mF_2(IRO)–h_mF_2(VS), from globally distributed measurements made during the period 11 April 2001 to 30 June 2002.

profiles. For the retrieved profiles to be considered, observations were required to 'coincide' spatially (cross-section diameter of up to 1600 km) and temporally (time window of up to 30 min). It was found that the majority of profiles agree well within the error ranges of both methods (Stolle et al., 2004). Beside the above-mentioned studies, comparison with reconstruction results from the Multi-Instrument Data Analysis System (MIDAS) algorithm was also performed. The algorithm is designed to assimilate data from a number of different measurement techniques, thus allowing the spatial and temporal factors to be accounted for during the inversion process. Various types of ionospheric data have been collected: International GPS Service (IGS) network data, true height profiles from vertical ionograms, Navy Ionospheric Monitoring System (NIMS) observations from Italy, etc. The experimental results proved an excellent agreement between the specification of ionospheric electron concentration using MIDAS and CHAMP IRO measurements (Spalla et al., 2003). Additionally, IRO profiles were compared with profiles from empirical models (e.g. IRI-2001)

in order to get some information concerning accuracy and reliability of the retrievals (Jakowski and Tsybulya, 2004).

2.4. Topside ionospheric scale height retrieval from IRO measurements

When the satellite orbit is well above the F2 layer peak, as in the case of the Oerstedt and SAC-C satellites, the comparatively small plasmasphere contribution can be considered to be constant. This simplifying assumption cannot be applied to the CHAMP IRO retrieval algorithms because CHAMP has a rather low orbit height of less than 450 km. Special care is required when determining the upper boundary condition at the CHAMP altitude, due to the fact that the above-lying ionosphere and plasmasphere can contribute up to an estimated 50% of the total signal (Jakowski et al., 1981, 1999). To overcome this problem, the inversion is assisted by an adaptive electron density model of the topside ionosphere and plasmasphere (TIP):

$$N_e(h) = N_mF_2 \exp\left(\tfrac{1}{2}(1 - z - \exp(-z))\right) + N_{PO} \exp(-h/H_{PP}), \quad (2)$$

where $N_e(h)$ is the electron density, $z = (h - h_mF_2)/H_{TI}$, N_mF_2 and h_mF_2 are the peak electron density and height, H_{TI} is the scale height in the topside ionosphere, H_{PP} is the plasma scale height in the plasmasphere, and N_{P0} is the electron density at the plasmasphere basis. The plasmaspheric scale height (actually, the H^+ ion scale height) increases gradually up until 10,000 km, above this altitude the scale height is assumed to be constant and its value is fixed to 10,000. In the occultation retrieval, the free parameters N_mF_2, h_mF_2 and H_{TI} are adjusted iteratively (currently the max number of iterations is limited to 6), starting from some plausible values. The iteration process delivers a 'smooth' transition from TIP electron densities to the values computed from IRO data. Ultimately, this procedure delivers the scale height at the upper boundary of the retrieved electron density profile. However, it should be stressed that in the here described procedure, due to the fact that we are using the Chapman ionospheric model (Davies, 1996) to assist the reconstruction of the topside ionospheric electron density profile and following the definition of the Chapman production function (Hargreaves, 1992), the so-called 'plasma scale height in the topside ionosphere' is closer to the neutral gas (atmospheric) scale height in the topside ionosphere rather than the real plasma scale height. Therefore, to avoid misunderstanding, we will further use the term 'topside ionospheric scale height' (denoted H_{TI}) or simply, scale height (H_{sc}). To get a rough estimate of the plasma scale height in the topside ionosphere, one should double the H_{TI}

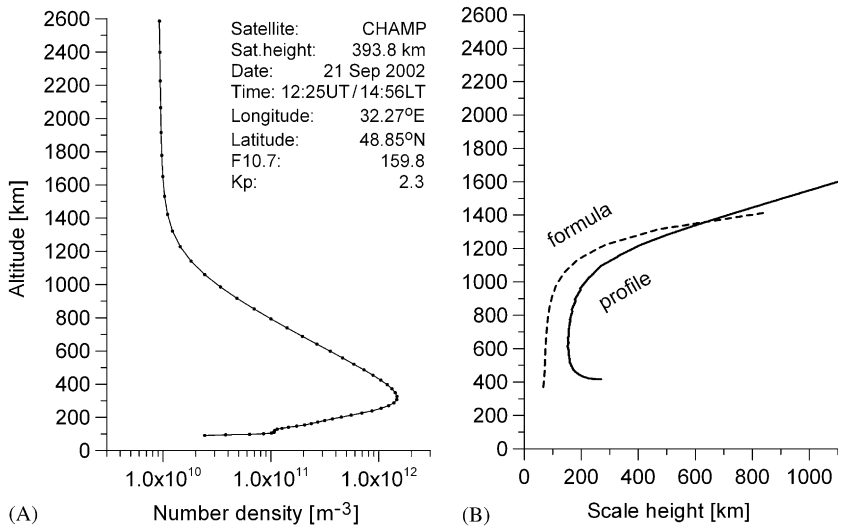

Fig. 5. An electron density profile retrieved from IRO measurements (Panel A); a vertical mesh of 88 irregularly distributed points is used for mapping the density in the altitude range from 90 km up to 20276 km. Panel B: the altitudinal variations of the plasma scale height as deduced directly from formula (2) and from the Ne profile.

value (if assuming thermal equilibrium). The reasons for using H_{TI} are the following. First, the 'profile-based' procedure fails to extract values near the h_mF_2 due to the curvature of the profile, while the formula-based method delivers. Second, the plasma scale height variations should be similar to the variations of the H_{TI} in the topside ionosphere. Finally, from the modelling aspect, it would be easier to apply the analysis of H_{TI} results into a model and then utilise the model directly into the initial guess in the reconstruction. Nevertheless, for validation of the plasma scale height, the best way will be to use the real plasma scale height (as extracted from the electron profile) and at the altitudes of the 'valley' of the scale height profile (Fig. 5), i.e. at an approximate altitude of 500 km.

The altitude range of the retrieved electron profiles (Fig. 5) is from 90 km up to the GPS height of about 20,000 km. A maximum of 450 IRO links are used for reconstructing the profile in the lower altitude range between 90 km and the CHAMP orbit height; the average number of mesh points in this range is 25. The distance between the mesh points increases with altitude; a total of about 90 mesh points are used for the entire altitude range. It is known that the distances between the mesh points in the plasmasphere can be larger with no significant decrease in numerical calculations; if necessary, suitable coordinate transformations can be applied (Stankov, 1990, 1996a).

3. Database

In this section we present the data set of topside ionospheric scale height values based on the CHAMP IRO measurements and some basic statistics. The database consists of measurements made in the period from 11 April 2001 until 31 March 2004. Within this period, 106,110 scale height values at altitude 425 km were successfully retrieved and sorted qualitatively (internal consistency check applied) into four classes (Fig. 6A). Out of this total number, 25,809 (or 24.32%) are classified as high quality, 57,790 (54.46%) as good quality, 13,822 (13.03%) as fairly good, and the remaining 8689 (8.19%) as poor. In this study, only the good and high quality data (total 83,599) are taken into account. During the measurements period, the solar activity (Fig. 6B) varied from high (monthly medians of index F10.7 reaching maximum values of 238 in year 2001) to low (F10.7 monthly medians falling below 100 in year 2004).

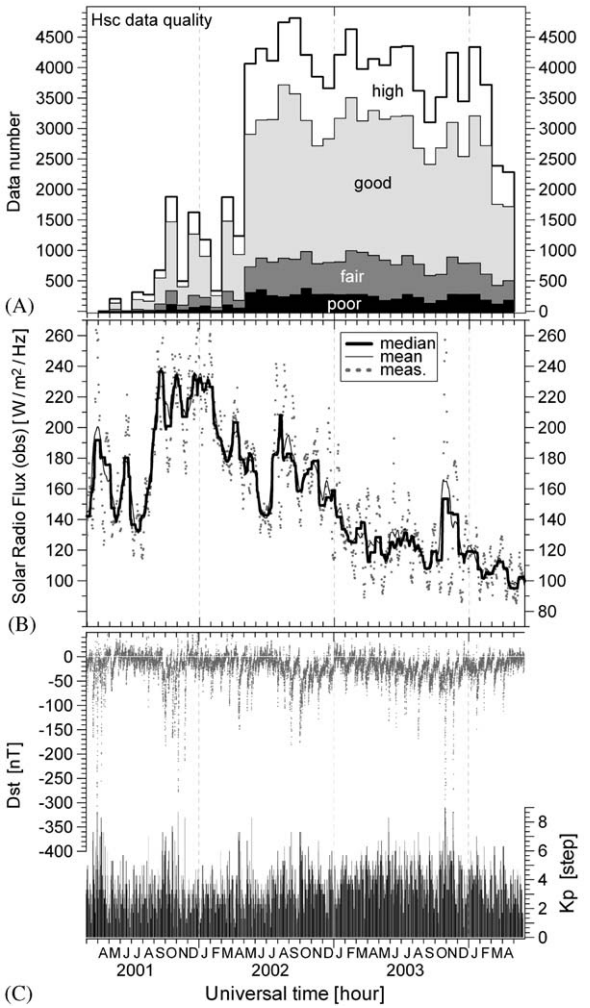

Fig. 6. Scale height database: data (quality and mission time) distribution (top panel) and the corresponding solar activity (middle panel) and geomagnetic (bottom panel) conditions.

Out of the large variety of solar activity indices currently available, we have chosen the F10.7 index since it is based on reliable measurements of the radio emission from the Sun at 10.7 cm wavelength (fluxes from the entire solar disc at a frequency of 2800 MHz in units of 10^{-22} J/s/m^2/Hz). Being a proxy for the background solar ultraviolet radiation flux, the F10.7 index is less noisy than the sunspot number index on a day-to-day basis. In addition, several measurements are made each day in order to remove the effects of short-term radio bursts. There are 3 sets of F10.7 values—observed, adjusted, and absolute. The observed values are least refined and contain the fluctuations that arise from the changing Sun–Earth distance. The adjusted values have this variation removed, meaning that these numbers

represent the energy flux received by a detector located at the mean Sun–Earth distance. An absolute number is obtained from an adjusted number but multiplied by 0.90 to compensate for uncertainties in antenna gain and in wave reflections from the ground (O'Loughlin, 1997). Here we use the observed values. The geomagnetic activity is also proven to affect the scale height behaviour, so to facilitate the analysis, we have also collected the K_p and D_{st} index values (Fig. 6C). Several major storms occurred in this time, clearly seen on the plot, marked by the extremes of both indices. Because the present study is focused on the average behaviour (climatology) of the scale height, only non-storm values are considered. For such non-storm scale height values we consider the values obtained when the current K_p index was 4 and less. In this way (Fig. 7B), further 11,042 measurements (13.2%) were discarded. Finally, the scale height database used in our study consists of 72,557 good/high-quality non-storm values.

When studying/analysing the behaviour of the ionospheric characteristics, the common approach is to present this behaviour against the following parameters (Taylor, 1971): solar activity, geomagnetic activity, season (day of year, DOY), LT, geomagnetic longitude, and geomagnetic latitude. The data distribution along the full range of each is available for all 6 parameters (Fig. 7). The distribution according to the solar activity index F10.7 (Fig. 7A) shows that the highest data number, of more than 8000, is in the 110–120 bracket. Almost half of the data (35,974, or 49.58%) lie in the medium solar activity range of [120,180], 18,182 (25.06%) are in the low solar activity range (F10.7 < 120), and the remaining 18,401 (25.36%)

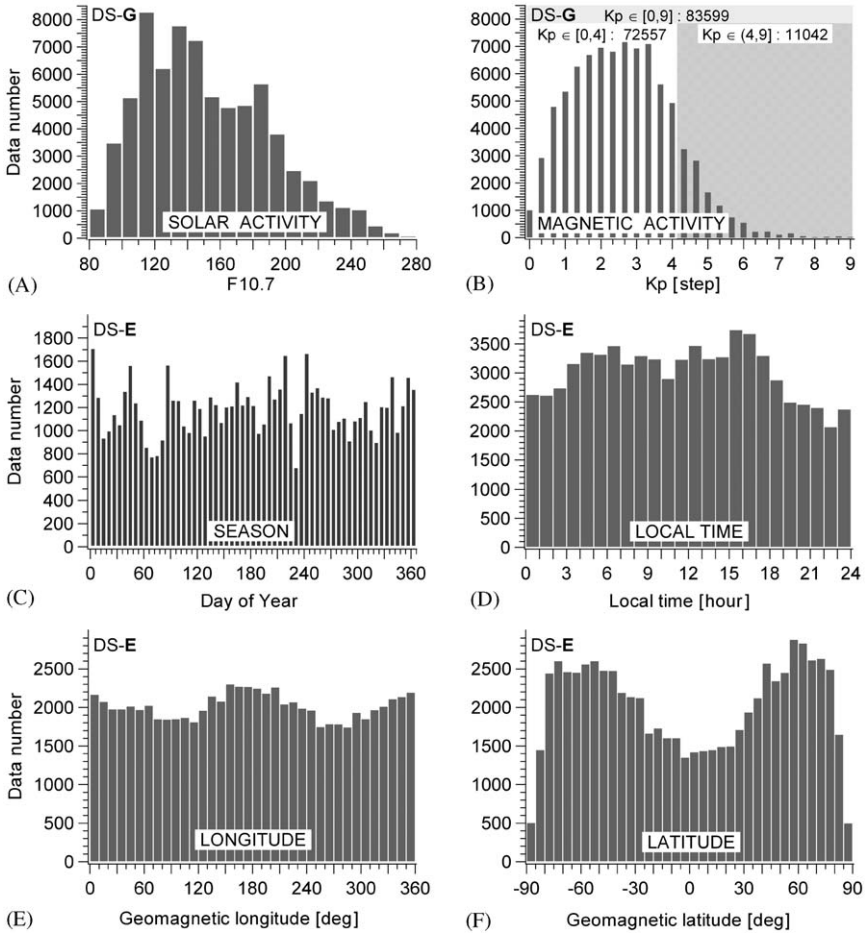

Fig. 7. Scale height database: data distribution according to solar activity (panel A, data set DS-G), geomagnetic activity (panel B, data set DS-G), season (panel C, data set DS-E), local time (panel D, data set DS-E), geomagnetic longitude (panel E, data set DS-E), and geomagnetic latitude (panel F, data set DS-E).

are in the high solar activity range of F10.7 > 180. It is interesting to see that extremely high readings of F10.7 > 250 were still accounted, despite the fact that measurements during $K_p > 4$ were already discarded (Fig. 7B). The high values of F10.7 combined with low values of K_p can be eventually explained with some characteristics of the ionosphere response to solar and geomagnetic forcing. The general understanding is that the active Sun is the primary driving force for increased geomagnetic activity (e.g. compare Fig. 6B and C) and the geomagnetic activity is thus related to the solar activity. In some solar cycles they vary together but in others they are less related to one another (Hargreaves, 1992). In the rising part of the solar cycle, the majority of the storms are thought to be caused by solar flares (or coronal holes near them), while in the decreasing part of the cycle there might be additional, even more influential factors. Thus, a tendency exists for the geomagnetic disturbances to peak once during the rising part and again (even stronger sometimes) during the decreasing part. To check the situation during the CHAMP mission, the number of geomagnetically disturbed days ($K_p \geqslant 4$) has been compared with the yearly averaged solar flux (Fig. 8). It is worth noting the huge number of disturbed days in 2003. Another important feature of the Sun–Earth relationship is the delayed ionospheric response to solar/magnetic activity forcing (Fuller–Rowell et al., 1994; Szuszczewicz et al., 1998; Kutiev and Muhtarov, 2001). The distribution according to season (actually, DOY is used here, data sorted in bins of 6 consecutive days, Fig. 7C), shows irregularly distributed data with minima around DOY 72 (less than 800) and DOY 231 (less than 700) and maxima around DOY 3 (more than 1700), DOY 219 and DOY 243 (more than 1600). The LT distribution (Fig. 7D) reveals higher number of data during the day (particularly in the early afternoon 1500–1700LT) and lower number during night (particularly in the late evening, 2200–2400LT). The data distribution according to geomagnetic longitude (Fig. 7E) is more or less even, slightly lower numbers are seen in the 70–120 and 250–290 sectors. The data distribution according to geomagnetic latitude (Fig. 7F) is uneven (although pretty symmetrical to the equator) with highest data number in middle and high latitudes, lower in the equatorial and low latitudes, and extremely low in the polar regions. Following the outcome of the above analysis, several data sets have been defined (Table 1), all of which will be used in the follow-on analysis of the topside ionospheric scale height behaviour.

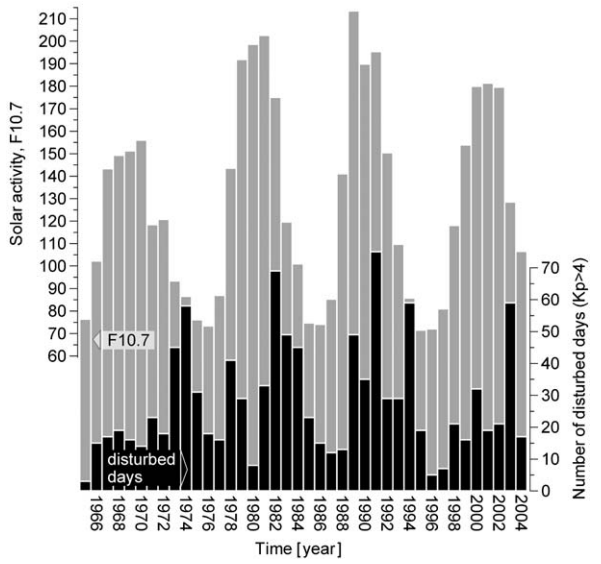

Fig. 8. The number of magnetically disturbed days, i.e. for $K_p \in (4,9]$, compared with yearly averaged values of the observed solar radio flux. Notice the phase shift, clearly seen at the maxima.

Table 1
Definition of the data sets used

Data set	Count	IRO quality	F10.7	K_p	Comment
DS-A	18,182	Good + high	180 +	[0–4]	High solar activity, non-storm data.
DS-B	35,974	Good + high	120–180	[0–4]	Medium solar activity, non-storm data.
DS-C	18,401	Good + high	−120	[0–4]	Low solar activity, non-storm data.
DS-D	11,042	Good + high	All	(4–9]	All solar activity, storm-time data.
DS-E	72,557	Good + high	All	[0–4]	All solar activity, non-storm data.
DS-F	33,992	Good + high	All	[0–2]	All solar, low magnetic activity data.
DS-G	83,599	Good + high	All	All	Complete, good- and high-quality data.
DS-H	106,110	All	All	All	Complete, least refined data.

4. Scale height behaviour

Understanding the ionosphere's natural variability and the mechanisms that give rise to it is very important if we are to be able to understand the behaviour of its main characteristics. However, the identification and precise interpretation of all physical phenomena and mechanisms that influence the behaviour of these basic ionospheric characteristics is a broad and complex subject which, considering the fact that the topside ionospheric height is one of these crucial characteristics embodying in itself the majority of the information/effect on the topside ionospheric composition and dynamics, is therefore very difficult to present in a single publication. However, while analysing the scale height behaviour, we will try to outline some of the physical mechanisms that are considered important in determining this behaviour.

Based on CHAMP IRO observations from the recent years, April 2001 until March 2004, important insights into the ionospheric scale height behaviour have been acquired for various solar and geomagnetic, diurnal, seasonal, longitudinal and latitudinal conditions. In order to better investigate the scale height behaviour according to each of these parameters, it was necessary to define seasons, day/night periods, and latitude ranges. For each hemisphere, the year has been split in three seasons—winter, equinox, and summer. Each season has been defined as a 91-day period centred on the corresponding solstice/equinox day (i.e. the 356, 81 and 264, 173 DOY) with respect to the opposite seasons in the Northern and Southern hemispheres (Table 2). Daytime conditions are defined from 0700 to 1700LT, and night-time are from 1900 to 0500LT. However, different day/night length is defined in the different seasons and latitudes: larger windows are used for extracting summer daytime and winter night-time data. It should be mentioned also that in general, the day/night definition is not well suited for the polar regions and thus, the results from both polar regions should be interpreted with caution as data can be mixed (daytime with night-time observations). To ensure that sufficient number of data is collected for the statistical analysis, the following 3 main geomagnetic latitude regions are defined—low $(-30^\circ, +30^\circ)$, middle $(\pm 30^\circ, \pm 60^\circ)$, and high $(\pm 60^\circ, \pm 90^\circ)$. In this way, the low-latitude region includes the equatorial region $(-15^\circ, +15^\circ)$ and the high-latitude region includes the polar areas. In some cases, however, in order to better investigate some regional phenomena, it will be necessary to treat the equatorial region separately from the common low-latitude region and the polar region separately from the aggregate high-latitude region. Considering the fact that the plasma density distribution in the topside ionosphere is mostly due to diffusion processes controlled by the geomagnetic field, and in view of easing the model development and implementation, we preferred the sorting and analysing of data to be performed with respect to the geomagnetic coordinates rather than the geographic coordinates. Nevertheless, the use of geomagnetic coordinates comes with some inconveniences, which should be noted. First, it is the definition of 'day' and 'night' for the high-latitude areas and corresponding treatment of the polar day and night. It is obvious that, due to the position of the geomagnetic poles, both the 'winter day' and 'summer night' selections may well contain H_{sc} values from both, dark and sunlit, parts of the ionosphere. For these cases, the notions 'day' and 'night' have rather symbolic meanings; plots will be denoted accordingly and the reader should be aware of higher probability of errors. Another inconvenience is the well known anomaly of the geomagnetic field which is such that in the sector around 280° geographic longitudes the field lines cross the geographic equatorial plane at altitudes that are

Table 2
Definition of the seasons: winter, equinox, and summer

	Winter	Equinox	Summer
North	DOY (solstice): 356 DOY: 311–365/6 DOY: 001–035	DOYs (equinox): 81, 264 DOY: 036–127 DOY: 219–310	DOY (solstice): 173 DOY: 128–218
South	DOY (solstice): 173 DOY: 128–218	DOYs (equinox): 264, 81 DOY: 219–310 DOY: 036–127	DOY (solstice): 356 DOY: 311–365/6 DOY: 001–035

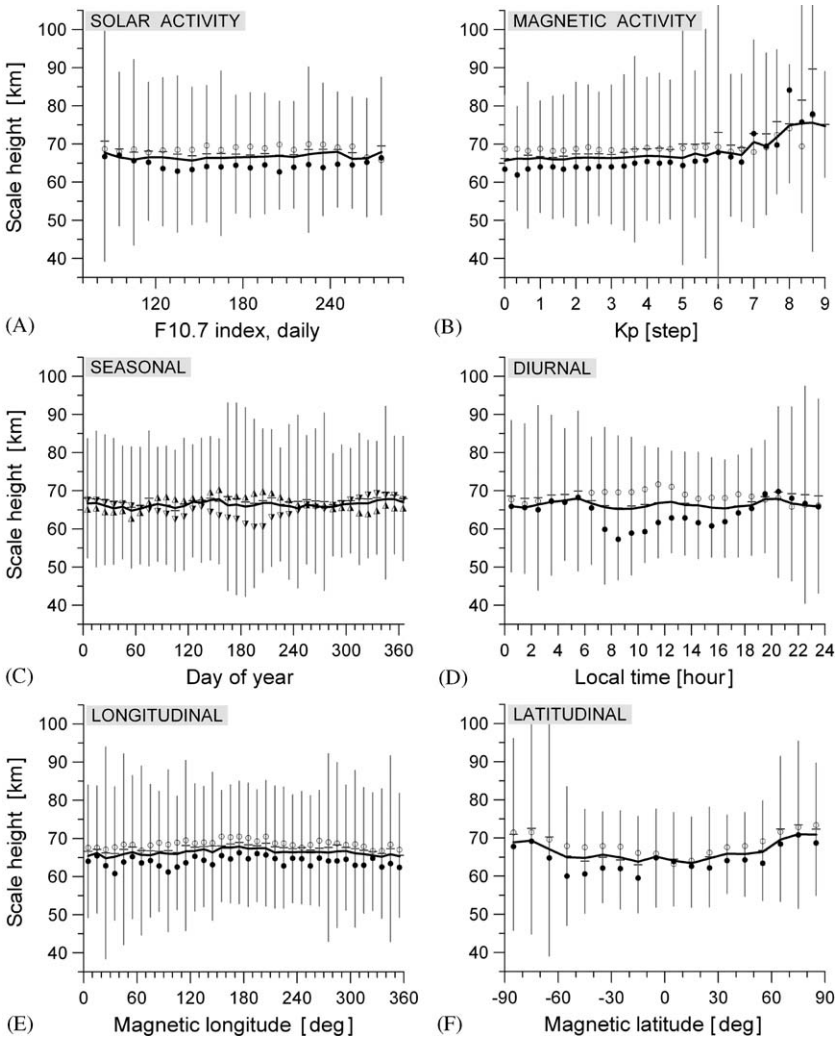

Fig. 9. Scale height variations (general) due to solar activity, geomagnetic activity, day of year, local time, longitude, and latitude (for the corresponding data distribution and data sets used, please refer to Fig. 7). The average scale height values denoted with horizontal bars, while the (doubled) standard deviations are given with vertical bars. The median values in each panel joined with a solid curve. The median value for each bin is denoted with a circle for summer conditions and a filled circle for winter conditions. To enhance the annual (seasonal) variations, the median values from the North hemisphere are differentiated from those from the South.

lower than the crossing points of the corresponding lines from other longitudes. Hence, in this sector, the inter-hemispheric flows are facilitated and large-scale alterations in the topside ionospheric structures become possible (Akasofu and Chapman, 1972; Van Zandt et al., 1972).

To get a first impression of the data distribution and the average behaviour, all measurements are plotted together (Fig. 9). Due to the large number of data from all sorts of different conditions, it is a bit difficult to detect particular trend in the average behaviour. An exception is the latitudinal behaviour which suggests an increase in poleward direction and a notably larger data scattering at high latitudes. The use of medians (rather than the averages) seems to be the better choice for the analysis here as the data scarcity in some regions may compromise the interpretation.

4.1. Dependence on solar activity

Theoretically, the total ionisation of the ionosphere is strongly affected by the solar EUV radiation ($10\,\text{nm} < \lambda < 130\,\text{nm}$) that causes the photoionisaton of the neutral gas. Since the solar radiation controls a complex magnetosphere–iono-

sphere–thermosphere system with quite different coupling processes, their characteristic time scales are difficult to separate. As said in the introduction, the ionospheric plasma scale height is directly proportional to the plasma temperature. Hence, given the well known dependence of the plasma temperature (T_P) on solar activity (Brace and Theis, 1978, 1981) and the strong correlation of T_P with the solar activity index F10.7, it is then expected that the scale height would also depend on solar activity and that an analysis of the scale height variations versus F10.7 index would be a good choice to investigate such dependence. To investigate how the IRO-deduced H_{sc} responds to solar activity, we have plotted the H_{sc} values against daily F10.7 solar flux observations with respect to season and day/night-time conditions for high, middle and low latitudes (Fig. 10) and geomagnetic non-storm conditions (data set used DS-E).

At middle latitudes (Fig. 10B), the seasons are well defined and well manifested, so we start the analysis with them; a quick look on the plots reveals significant LT and seasonal differences. During the day, in summer and equinox, the scale height increases in line with the F10.7 index. The increase is not so strong but is present throughout the whole F10.7 range. The situation changes in daytime winter, when a negative (decreasing) trend is observed during low solar activity, when H_{sc} decreases from 60 km down to about 50 km, and oppositely, a strong positive trend is observed for high solar activity (F10.7 > 150) when H_{sc} rises from 50 km up to about 70 km. On average, the H_{sc} increases from winter to summer. During the night, the median H_{sc} values remain more or less constant. The drop in H_{sc} for F10.7 > 200 in night-time summer can be attributed to the low number of data and/or limitations in the accuracy of measurements. In night-time winter, a small but steady decrease of H_{sc} is noticed for F10.7 < 200 and an H_{sc} increase for F10.7 > 200. Nevertheless, during night time the H_{sc} on average decreases from winter to summer, which is just opposite to day time.

At low latitudes (Fig. 10C), although the data scattering is a bit higher, both the day- and night-time behaviour of H_{sc} resembles that at middle latitudes. The interesting trend during winter is again preserved; however, the dip at F107 = 135 is not so pronounced. At high latitudes (Fig. 10A), only night-time winter and daytime summer variations of H_{sc} are plotted in order to avoid interpreting results mixed day/night conditions. The median H_{sc} obviously experiences no major changes during summer. This is not the case in winter: H_{sc} decreases from a maximum of about 100 km (at F10.7 = 80) to minimum values of about 65 km (at F10.7 > 180), a dive of more than 50%.

The relatively short period of accumulating IRO data impedes the proper investigation of the solar activity dependence, particularly at low and high solar activities. As seen from the plots, the majority of measurements are in the middle activity range of F10.7 between 120 and 180, and for this reason we limit our further analysis to data from this activity range only. Also, for higher precision in the determination of the scale height, the question of possible time delay of the H_{sc} response to solar radiation changes should be investigated. Correlative studies between GPS TEC and the daily solar radio flux show delays of the ionospheric response to solar radiation; moreover, the response seems to be latitude dependent—from about 1 day at 35°N up to about 3 days at 65°N (Jakowski et al., 2002a). Another useful shape parameter is the upper ion transition level (UTL); the latter has been found to significantly increase in line with the solar activity (Kutiev et al., 1994; Kutiev and Stankov, 1994; Stankov, 1996b, 2002a). The UTL behaviour, combined with the F2 peak response to solar activity can provide important clues on the topside ionosphere scale height behaviour.

4.2. Dependence on geomagnetic activity

During the years, thanks to meticulous observation and simulation work, advanced understanding of the geomagnetic/ionospheric storms has been acquired, and many evidences have been accumulated as to the effects of ionospheric/magnetic storms on the processes occurring in the F2 layer and on the shape of the topside density profiles above the F peak (Matsushita, 1967; Mendillo et al., 1975; Fuller-Rowell et al., 1994, 2000; Proelss, 1995; Buonsanto, 1999; Foerster and Jakowski, 2000). However, most of the work was on other characteristics related to the ionospheric scale height, such as N_mF_2, h_mF_2, and TEC, rather than directly on the scale height.

At high latitudes, the plasma density structure during geomagnetic storms experience perturbation changes due to magnetospheric drivers, such as intensified convection electric fields and enhanced energetic particle precipitation (Parkinson and Hutton, 1989). As a result, the auroral zone expands

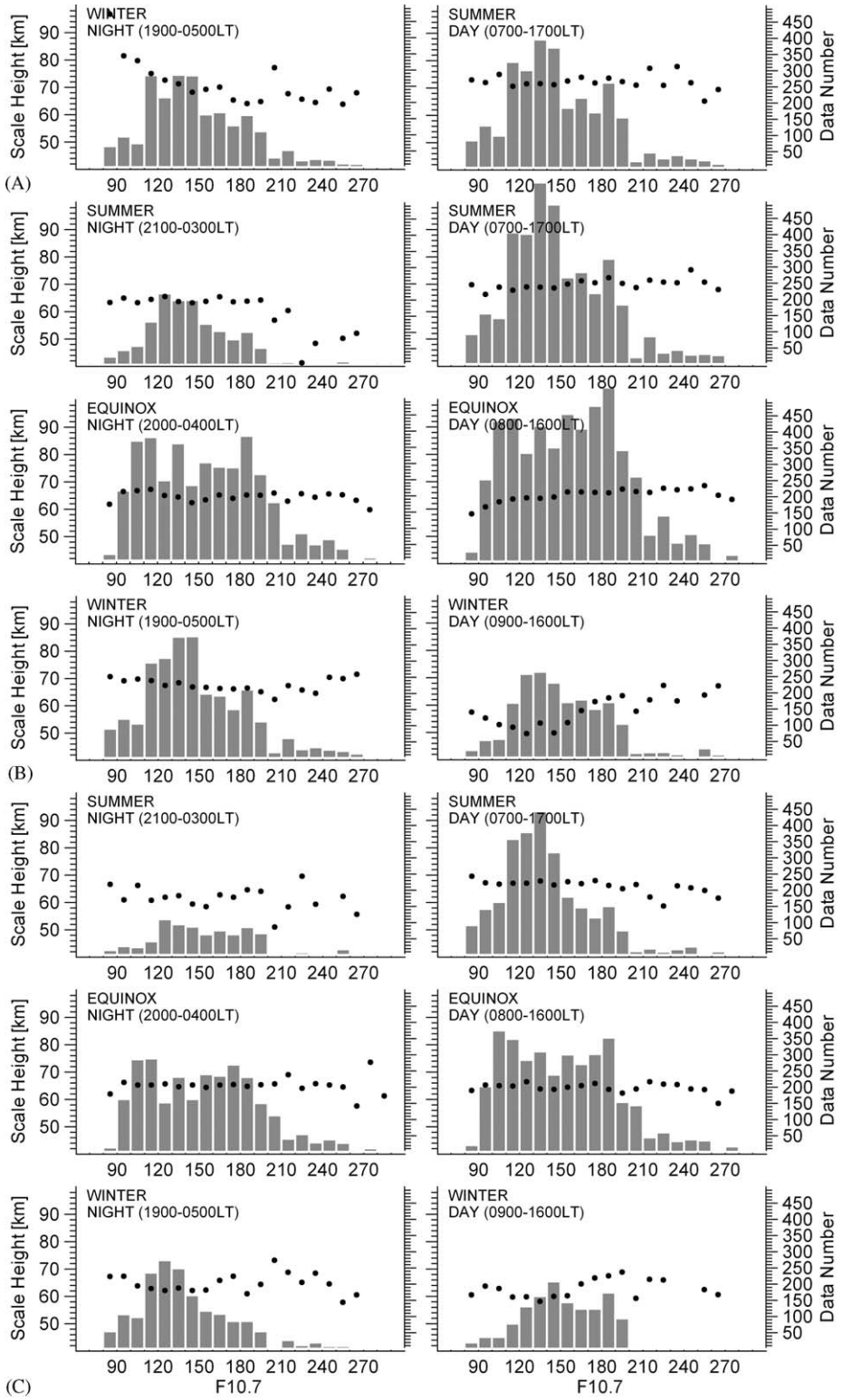

Fig. 10. Scale height dependence on solar activity: panel A—high latitudes ($\pm 60^\circ$, $\pm 90^\circ$), panel B—middle latitudes ($\pm 30^\circ$, $\pm 60^\circ$), and panel C—low and equatorial latitudes (0°, $\pm 30^\circ$). Data set: DS-E.

significantly, accompanied by several phenomena such as occurrences of deep ionisation troughs, enhancements in electron temperature, plasma outflows, etc.

At middle latitudes, the F layer critical frequency (i.e. N_mF_2) is usually depressed during storms while at equatorial latitudes it usually increases. The general perception is that N_mF_2 and h_mF_2 behave in unison during geomagnetic storms. Thus, a rise in the F2 peak height to regions of reduced loss due to equatorward winds would also increase the F2 peak density; similarly, a dip in h_mF_2 due to poleward winds will reduce N_mF_2. In this way, due to LT variations in the neutral atmosphere composition/winds, at middle latitudes the negative storm effects are more often observed in summer and in the morning sector, while the positive effects prevail (and last longer) in winter and in the afternoon/evening sector. It should be noted, however, that there are reported cases of storms during which a sustained increase in h_mF_2 is observed accompanied by a strong decrease in N_mF_2 in comparison with previous quiet days, the latter explained with negative storm effects caused by neutral composition and temperature changes (Proelss, 1995; Mikhailov and Schlegel, 1998).

The electron density structure in the low latitude and equatorial ionosphere is well known to be dominated by the vertical $E \times B$ drifts which drive the equatorial fountain effect. The low latitudes respond quickly to an increase in geomagnetic activity by accelerating the downward $E \times B$ drift perturbation in the post-midnight and early morning hours and the reverse upward drift in the remaining hours. Even under geomagnetically quiet conditions, the plasma density distribution at low latitudes is extremely volatile, particularly between dusk and midnight hours, due to the presence of irregularities. These unstable conditions may result in larger Ne gradients. Therefore, how the geomagnetic storms affect the ionospheric scale height depends on how the equatorial irregularities develop during storm—a difficult question considering that those irregularities vary with longitude and from storm to storm.

One of the crucial findings is that the ionosphere–plasmasphere behaviour during geomagnetic storms is tightly connected to the concurrent thermospheric storms via changing production/loss rates and generated electric fields redistributing the plasma. This mechanism can explain the observed behaviour in the storm on 10 April 1990 (Fig. 11).

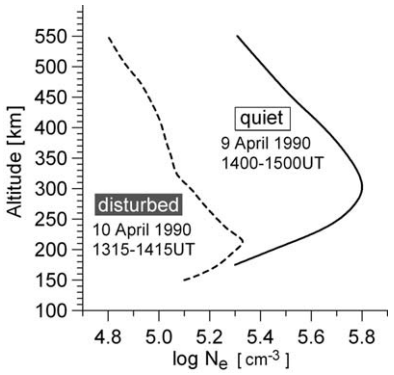

Fig. 11. Electron density profiles observed at EISCAT for various quiet and disturbed conditions (after Mikhailov and Foster, 1997).

In the presented case, the peak density and peak height both decreased severely during the storm; in fact, the F2 layer disappeared completely and the peak actually shows the F1 layer. As a result, the H_{sc} in the topside ionosphere increased significantly which is obvious when comparing the disturbed profile with the corresponding density profiles from the previous (quiet) day. The observed depletion can be explained (Buonsanto et al., 1992; Mikhailov and Foster, 1997; Mikhailov and Schlegel, 1998; Pavlov et al., 2000) with severe perturbations in ion composition (the $n(O^+)$/Ne ratio), decrease in thermospheric quantities (the $n(O)/n(N_2)$ ratio), and large increase (several hundreds degrees) in the exospheric temperature. The experience leads to the conclusion that the neutral composition and temperature have a major impact on the storm-time behaviour of H_{sc}. It also provides an example of how the ISR measurements can be used to deduce the plasma scale height.

One of the factors influencing the TEC, and from there the scale height behaviour, is the large-scale ionospheric perturbation observed during geomagnetic storms. To understand the complexity of such large-scale perturbation, correlative studies have been carried out and the results indicate that horizontal TEC gradients are definitely correlated with the geomagnetic activity (Fig. 12). In agreement with the occurrence distribution of horizontal TEC gradients, the large-scale gradients enhance with the level of ionisation, i.e. the highest gradients are observed at daytime. Furthermore, it is evident from the figure that perturbation-induced gradients are stronger in latitudinal than in longitudinal direction.

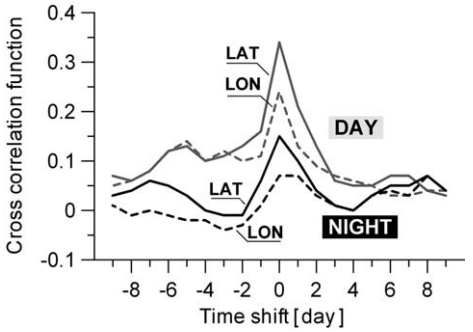

Fig. 12. Cross-correlation between latitudinal and longitudinal TEC gradients and the 3-h ap index for data sets taken from European TEC maps that cover the years 1995–1999.

The IRO measurement experience is also promising. Valuable information about geomagnetic storms have been supplied by the GPS radio occultation experiment onboard the CHAMP satellite. When a GPS satellite crosses the Earth limb and is seen from CHAMP through ionospheric layers, the GPS receiver measures differences between signal phases and pseudoranges on two frequencies of the GPS signal. These differences arise because of the dependency of the wave's phase and group speed on the ionospheric plasma density and can be used to determine the slant TEC value, i.e. the integral of the electron density along the line of sight between the GPS transmitter and the CHAMP receiver. Presented here (Fig. 13) are a few profiles of the differential TEC versus occultation time together with the corresponding inversed vertical profiles of electron density from the disturbed period in November 2001. The occultation sites (the sites, where the GPS–CHAMP raypath touched the Earth surface) were located at middle latitudes. During the first occultation event (panel A) performed before the storm, no irregular features were seen, while, after the storm started, the plots show strongly enhanced TEC and Ne profiles (Panel B) during the main phase, and a seriously depleted F region (Panel C) during the recovery phase. Our studies indicate that ionospheric irregularities are quite common during storms even at middle latitudes, and that the IRO technique is very useful in monitoring these irregularities (Jakowski et al., 2005a). It is also important to mention that the IRO-retrieved electron profiles during magnetically disturbed conditions show that the behaviour of the topside ionospheric scale height is not uniform and may increase in some cases but decrease in others.

In order to better reveal the scale height dependence on geomagnetic activity, we have chosen to use the K_p index because of its easier interpretation (Mayaud, 1980; Menvielle and Berthelier, 1991) and good representation of the storm-time ionosphere changes (Della-Rose et al., 1999). For this purpose only, the 'K_p-complete' data set (DS-G) has been used. It became clear from the selection results (Fig. 14) that during storms (i.e. when $K_p > 4$) the scale height tends to increase. However, the data are scarce for $K_p > 6$ (the data number is less than 10 for any K_p step above 6), so some caution must be observed until results confirmed with additional IRO data and/or independent measurements.

At high latitudes, the scale height increases in line with K_p both during winter and summer. The storm-time data are relatively scarce and widely scattered, suggesting that the scale height may increase in some cases but decrease in others. At middle latitudes, the behaviour during daytime tends to be differing from night-time. During the day, H_{sc} increases steadily with K_p—more during winter (~25%) and less during summer (less than 10%). During night-time, H_{sc} remains more or less the same, except during storms when H_{sc} tends to increase, particularly at winter (Fig. 15). At low latitudes, the H_{sc} seems to be unaffected by geomagnetic activity with median values remaining almost the same.

It is difficult to fully cover in one paper all mechanisms that contribute to the H_{sc} behaviour during geomagnetic storms. Moreover, given the relatively limited IRO database it would be very difficult (at this stage) to precisely analyse and properly simulate the geomagnetic activity influence on H_{sc}. Therefore, further in this study we confine our efforts to non-storm conditions only ($K_p \leqslant 4$).

4.3. Dependence on season (annual variations)

As far as the ion/electron temperatures both experience significant seasonal variations it is natural to expect significant changes in the scale height also. Indeed, such changes are clearly observed in the accumulated data set. To better account for eventual hemispheric differences the results from the Northern hemisphere (Fig. 16) are plotted separately from the results from the Southern hemisphere (Fig. 17). It is immediately seen from the plots that the data in the selected LT windows are irregularly distributed during the year.

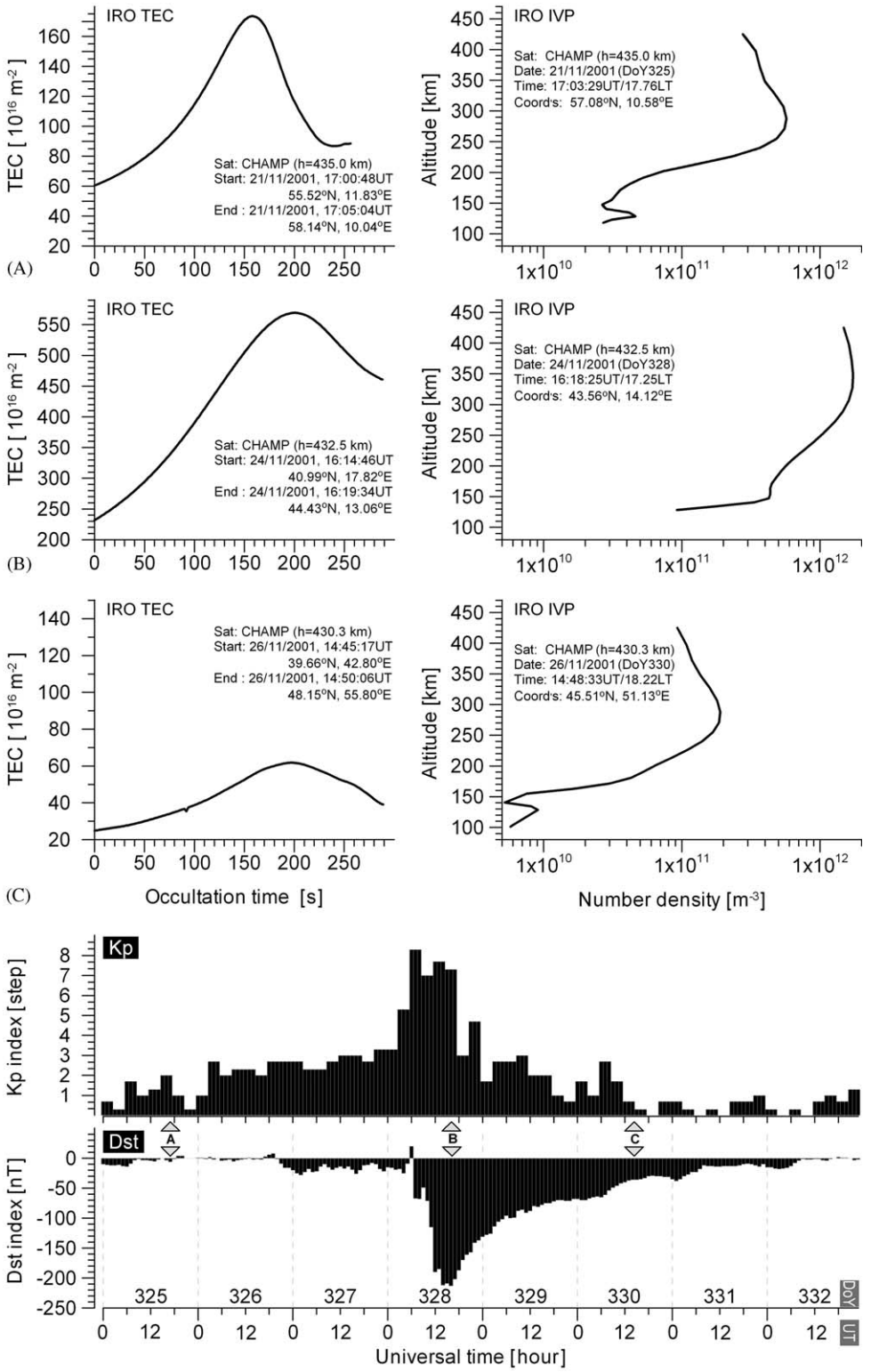

Fig. 13. Samples of the relative TEC (left panels) as measured along the radio occultation ray path and the corresponding electron density profiles (right panels)—during quiet (top panel) and disturbed magnetic conditions.

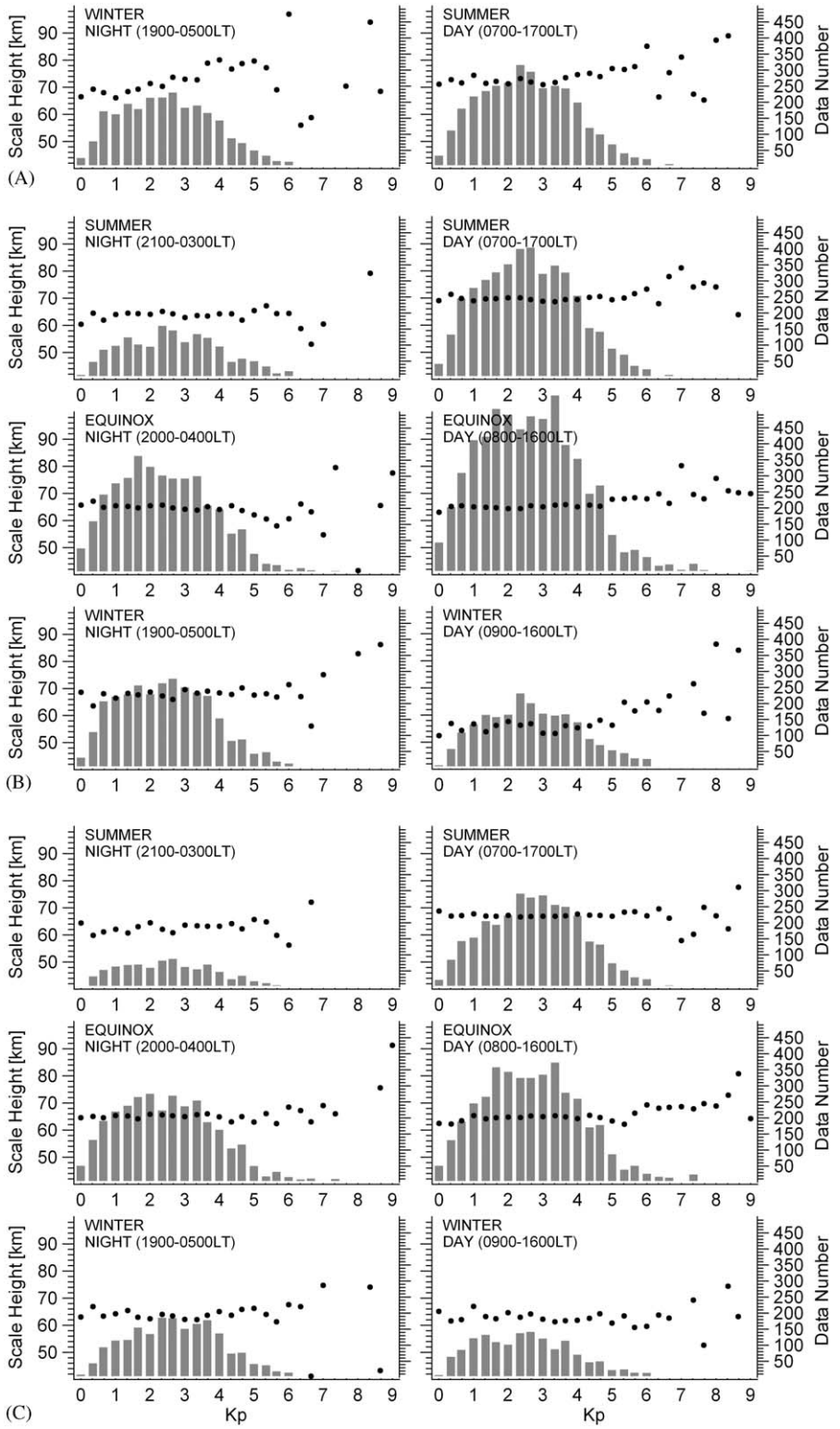

Fig. 14. Scale height dependence on geomagnetic activity: panel A—high latitudes ($\pm 60^\circ$, $\pm 90^\circ$), panel B—middle latitudes ($\pm 30^\circ$, $\pm 60^\circ$), and panel C—low and equatorial latitudes (0°, $\pm 30^\circ$). Data set: DS-G.

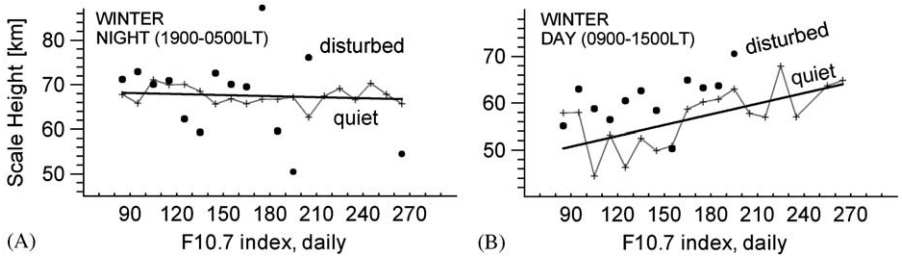

Fig. 15. Scale height dependence on solar activity during quiet (Kp∈[0-2], data set DS-F) and disturbed (Kp∈[4-9], data set DS-D) magnetic activity, in night-time (panel A) and day-time (panel B) winter conditions at middle latitudes.

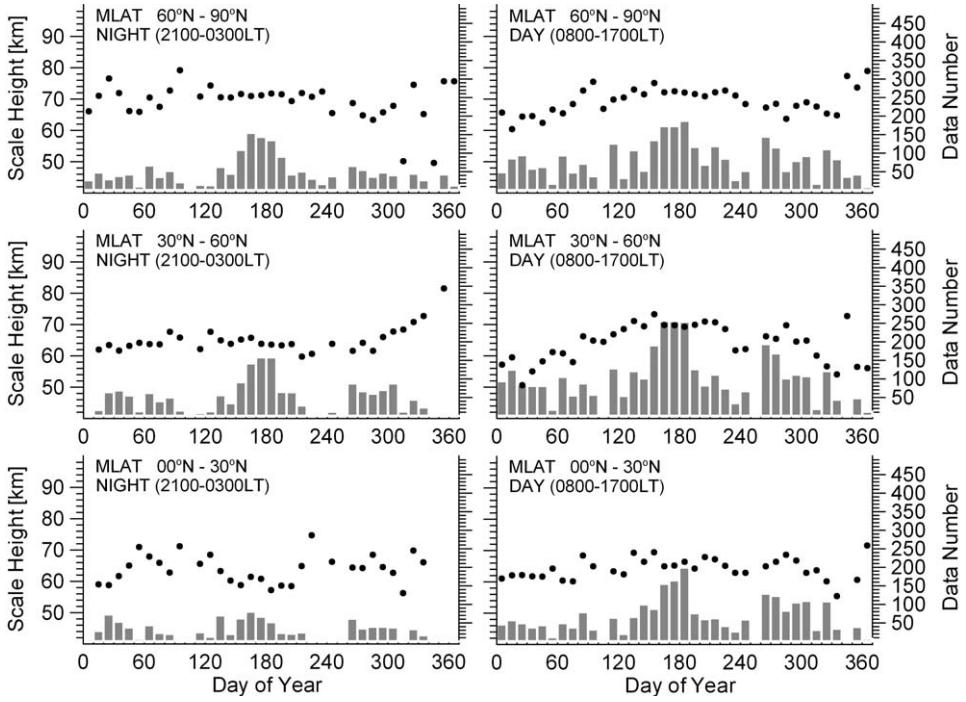

Fig. 16. Scale height dependence on season (Northern hemisphere): H_{sc} vs. DOY.

The majority of the measurements are clustered in the 140–220° and 260–300° longitude; more data have been assembled during day, particularly in the morning and evening hours (Fig. 7). During night (Figs. 16 and 17, left), medians show no clear evidences of significant seasonal differences. Data scattering is rather large and it is difficult to draw conclusions at this stage. On average, the medians increase with latitude. During day (Figs. 16 and 17, right), medians however, the seasonal changes are large and hence, are far more evident. All summer-time values are much higher than the winter-time values. The strongest seasonal differences are observed at middle latitudes. In the Northern hemisphere the winter-time minimum is at 51 km and the summer-time maximum is at 74 km, or about 45% difference. In South, the difference is even larger—the winter-time minimum is at 47 km and the summer-time maximum is at 71 km, quite an impressive increase of 57%. And if the differences in the median values are so large, one should certainly expect even larger differences in the individual values. In daytime, the latitudinal increase is again preserved.

4.4. Dependence on local time (diurnal variations)

Theoretically, being directly proportional to the plasma temperature, the plasma scale height is expected to be higher during the day and lower

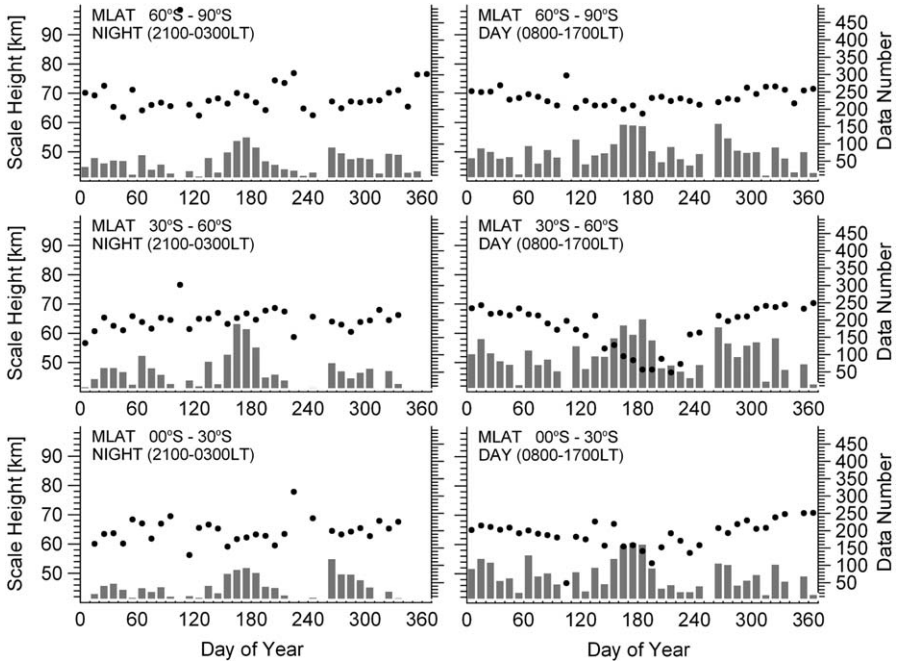

Fig. 17. Scale height dependence on season (Southern hemisphere): H_{sc} vs. DOY.

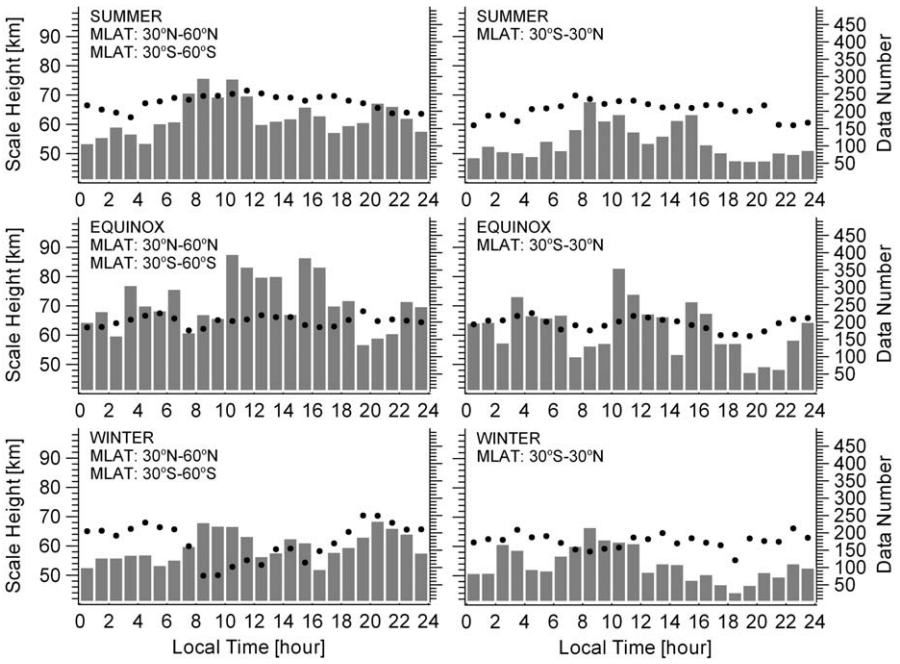

Fig. 18. Scale height dependence on local time: at middle latitudes ($\pm 30^\circ$, $\pm 60^\circ$), left panels, and at low latitudes ($0^\circ, \pm 30^\circ$), right panels.

during the night. This is definitely true during summer (Fig. 18, top panels) when H_{sc} rises from 60 km during night up to about 70 km during day. At high latitudes (above 60°), however, this pattern is lost and no significant variations are observed due to the short or absent night-time conditions. Thus, the values represent daytime conditions only and are about 72 km on average, i.e. slightly higher than

the daytime values at lower latitudes. In the other seasons—equinox (Fig. 18, middle panels) and winter (Fig. 18, bottom panels)—however, the behaviour is quite different. During equinox, starting from the background night-time values, H_{sc} increases in the early morning hours, decreases to a minimum around 0800LT, increases again to a midday peak, decreases in the afternoon, and finally, increases to the night-time values. At low-to-middle latitudes (20–45°), an evening increase some time between 1900 and 2000LT is also observed. The situation is, again, different in the middle-to-high latitudes (45–75°) in winter. Although the winter-time behavioural pattern shows similarities with the equinox behaviour, there are important differences too. First, a more detailed (latitude bins narrowed) look on the data confirms the existence of a pre-dawn enhancement (PDE) and post-sunset enhancement (PSE). Also, a strong correlation with slab thickness measurements at middle latitudes is detected (Fig. 19). Second, the morning/pre-noon decrease is quite sharp (values dive more than 30%) to an absolute minimum somewhere below even the 50 km mark. Actually, the drop is so strong that the H_{sc} cannot quite well recover throughout the day and as a result, the daytime values remain significantly lower than the night-time values. In addition, the evening peak at 1900LT is much more pronounced and prolonged until 2100LT.

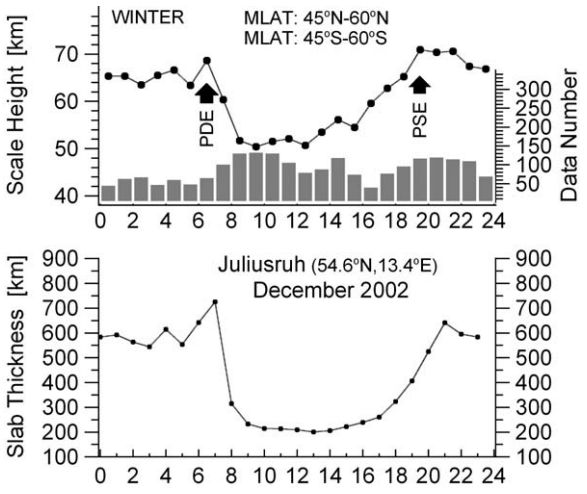

Fig. 19. Comparison between the diurnal behaviour of the plasma scale height and the slab thickness at middle latitudes during winter. Slab thickness calculated at the site of ionosonde station Juliusruh (54.6°N, 13.4°E) using foF_2 measurements from the Juliusruh digisonde and TEC measurements from IGS.

Several theories can be put forward to explain the above-described observations. The pre-dawn increase is a phenomenon closely related to the maintenance of the night-time F layer (Hanson and Patterson, 1964) and can sufficiently well be explained by the lowering of the ionospheric F layer immediately before sunrise to regions of greater neutral density, leading to increased ion loss due to recombination. The effect is believed to be particularly strong (Rastogi, 1988; Moffett et al., 1992) on the lower side of the F layer which also includes the F density peak. As a result, the decrease in NmF and bottom-side density is much faster than the topside ionosphere where the loss rate is lower. Thus, an enhancement in the topside scale height occurs. In addition, plasmaspheric fluxes can also play a role in the increase.

The pre-dawn increase can also be explained with the morning increase (overshoot) of the electron temperature (Oyama et al., 1996, 1997) which, being by definition related to the plasma scale height, causes a corresponding increase in the latter. Unfortunately, due to limitations in the Hinotori satellite orbit, the measurements are confined to low and equatorial latitudes only, and thus, the overshoot is proven for those latitudes. However, it is reasonable to expect similar increase at higher latitudes although not of the same magnitude. Another way to explain the PDE is to consider the fact that during sunrise a flux tube is being illuminated by the Sun from the top first which is causing advanced ion production in the TIP earlier than at low altitudes thus making the topside profiles temporary steeper. Additional contribution to the PDE can be provided via photoelectron heating. The question about the observed evening increase in H_{sc} remains more or less open. In our measurements, the PSE is well pronounced at middle latitudes and a reasonable explanation for such enhancement is the occurrence of plasmaspheric fluxes (Bailey and Sellek, 1992).

In search of confirmation and possible explanation of the above-described plasma scale height behaviour, we have compared H_{sc} and slab thickness measurements for corresponding conditions. By definition (Davies and Liu, 1991; Fox et al., 1991), the slab thickness τ is the ratio between TEC and N_mF_2, i.e. $\tau = \mathrm{TEC}/N_mF_2$, where TEC is the total electron content (electrons/m^2) and N_mF_2 is the F2 peak electron density (electrons/m^3). In other words, the slab thickness is the depth of an idealised ionosphere which has the same TEC as the actual

ionosphere but uniform electron density equal to the maximum electron density of the actual ionosphere. The slab thickness, measured in units of distance (usually, km), contains information on the neutral and ion gas temperature (Titheridge, 1973), and because it includes additional information from TEC observations which is not readily deducible from foF_2 observations alone, it therefore delivers information on both the top- and bottom-side ionosphere. Although the physical meaning of τ is not very clear, it is also related to the shape of the electron density profile as the scale height and thus is a very useful parameter linked to the scale height (Furman and Prasad, 1973). To check this correlation (and verify the scale height behaviour) compared here are plasma scale height and slab thickness measurements (Fig. 19). For this purpose, median values of the winter-time scale height are plotted together with corresponding slab thickness estimations at the site of the ionosonde station Juliusruh (54.6°N, 13.4°E) which is in the same mid-latitude belt. As seen from the figure, the correlation is very strong. It is important to mention here that independent measurements have been used for computing the slab thickness—TEC is obtained from the IGS measurements and N_mF_2 is derived from ionosonde measurements. Interestingly, our previous calculations show that such winter-time behaviour, of both H_{sc} and τ, is preserved for low solar activity levels as well. It is clear from the results that during quit-time conditions the slab thickness is correlated with the plasma scale height, whereas under disturbed conditions, the compression/expansion of the EDP is controlled mainly by dynamic forces such as neutral winds and electric fields. Most of the mechanisms determining the plasma scale height are valid for the slab thickness behaviour as well. Sharp changes in the slab thickness can be attributed to physical processes such as plasma uplifting, enhanced plasma fluxes from/to the plasmasphere, etc. (Foerster and Jakowski, 2000; Jodogne and Stankov, 2002).

Overall, our results suggest that the H_{sc} diurnal behaviour is much more complex than earlier anticipated, and that H_{sc} might not be so tightly correlated with the plasma temperature. It will be interesting to check a hypothesis of a possible strong positive correlation between the scale height (eventually the slab thickness) and the electron temperature during summer and weaker correlation during winter.

4.5. Dependence on longitude (longitudinal variations)

There are evidences that the ionospheric F region experiences noticeable differences along geographic/geomagnetic longitude mainly due to the characteristics of the geomagnetic field (Su et al., 1996). For example, ion composition observations onboard satellites revealed significant longitudinal variation in the composition of the topside ionosphere in the form of shift in the latitudinal distributions of the major topside ions. Both the location and prominence of distinct ionospheric features, including the O^+–H^+ transition level are found to vary significantly between longitudes for which the angle between the Earth–Sun line and the dipole equator has its greatest variation (Taylor, 1971). In addition, diurnal, latitudinal, and longitudinal variations of both the plasma density and composition, in combination with the zonal and/or meridional neutral winds, cause (even during geomagnetically quiet days) pronounced increase of Te in the morning hours and differences of Te between different longitude zones, between different seasons and hemispheres (Su et al., 1994; Oyama et al., 1996, 1997). In summary, it is natural to expect longitude differences in the shape of the electron profiles and from there to have changes in the scale height. Our results, however, show no indication of major geomagnetic longitude differences, neither at middle latitudes (Fig. 20) nor at high or low latitudes (Fig. 21). Only at middle latitudes during winter daytime, extremely low values are observed in the (330°E, 40°E), (190°E, 200°E), and (270°E, 290°E) longitude zones and oppositely, higher values are observed around 120°E. The whole picture, however, looks a bit chaotic, and considering the pretty low number of data, it would be quite difficult to try to explain the situation. Following this outcome, we have ignored the eventual existence of longitudinal variations when analysing the other types of variations.

4.6. Dependence on latitude (latitudinal variations)

In order to deduce the latitudinal behaviour of the plasma scale height, both night- and daytime all-longitude measurements have been sorted according to season (Fig. 22). During night-time, the plasma scale height tends to increase at higher latitudes. The increase is most obvious in summer, when the median values range between 60 and 74 km.

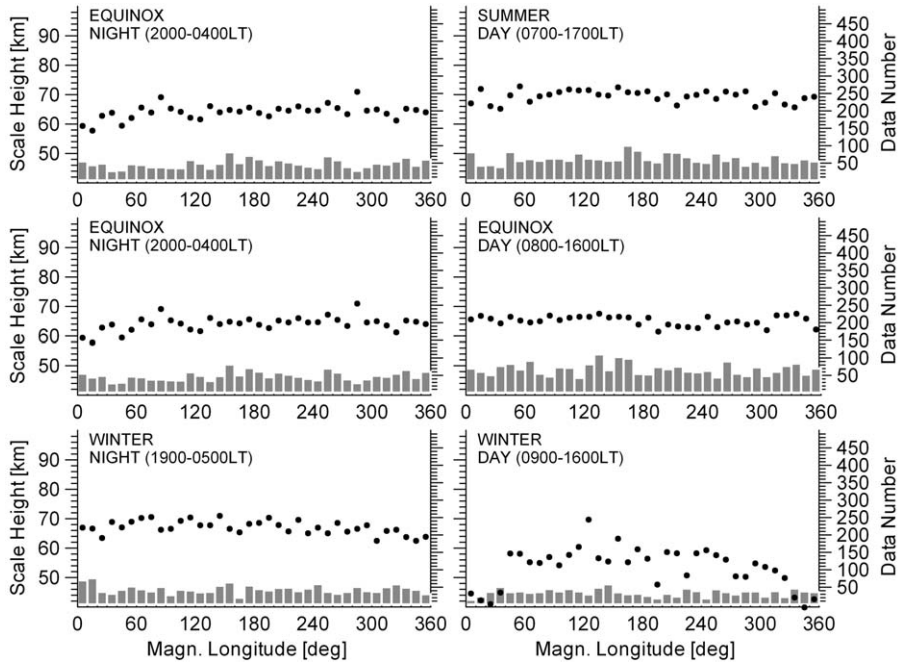

Fig. 20. Topside plasma scale height deduced from CHAMP IRO measurements. Observed longitudinal variations at middle latitudes ($\pm 30^\circ$, $\pm 60^\circ$).

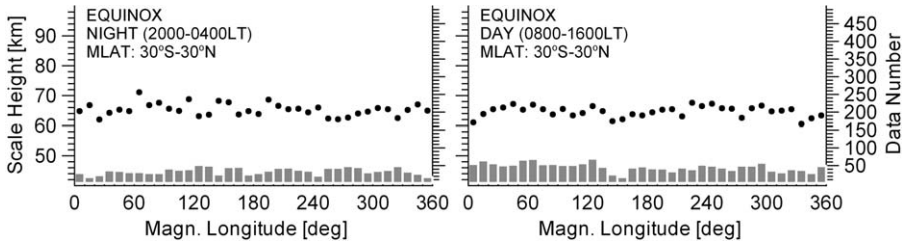

Fig. 21. Topside plasma scale height deduced from CHAMP IRO measurements. Observed longitudinal variations at low and equatorial latitudes (0°, $\pm 30^\circ$).

However, as mentioned before, the data from the polar regions may be 'contaminated' with daytime values, the latter have been showed to be higher. In this sense, it is more natural to have lower values at the poles (like the winter night-time plot shows) or at least the same (like the equinox plot). A more detailed treatment of the polar ionosphere measurements is required after we obtain more data. During daytime, the latitudinal increase is generally preserved, but with a few exceptions. At equinox, the values increase from 63 to 70 km. At summer, the scale height is higher—it averages 65 km over the equator and increases up to the record 74 km over the poles. An interesting case is the winter-time distribution—the median values in the equatorial region are around 68 km and are of the same magnitude as the median values over the poles. At the same time, a pronounced decrease is observed in the 45–55° latitude belt where the scale heights drop even below the 50 km mark. This phenomenon is probably due to the ion trough and/or serious violation of the diffusive equilibrium conditions, e.g. when strong vertical plasma fluxes occur (Jakowski et al., 1981). The main ionospheric trough occurs at—and is actually considered as—the boundary between the high latitudes and middle latitudes. It is characterised with abrupt gradients in electron density within relatively short horizontal distances. The depth, shape, location and extent of the trough depend on all/some of the usual suspects—solar and geomagnetic activity, LT, season, latitude and longitude.

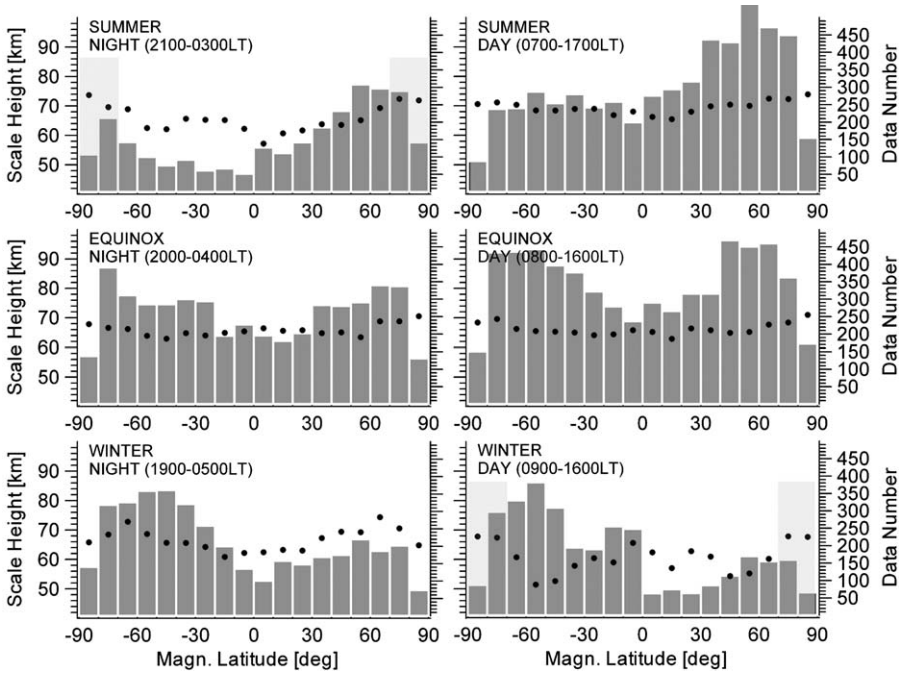

Fig. 22. Topside plasma scale height deduced from CHAMP IRO measurements. Observed latitudinal variations in winter (bottom), equinox (middle), and summer (top), during night-time (left) and daytime (right) conditions. Solar activity range F10.7$\in$ [120,180]. The light-grey areas in the plots indicate possibility for the polar regions to contain data from both dark and sunlit parts of the ionosphere/plasmasphere.

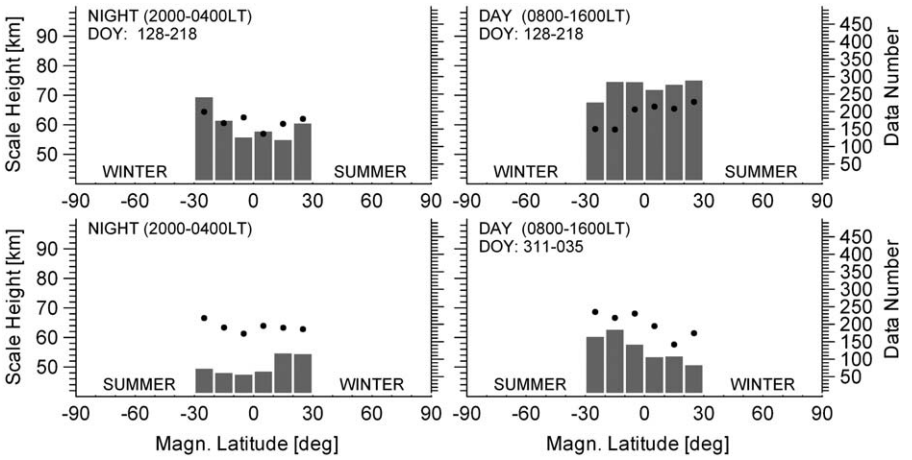

Fig. 23. CHAMP IRO topside plasma scale height: observed latitudinal variations at low latitudes (0°, $\pm$30°).

In order to better understand the seasonal and latitudinal changes in the equatorial area, we have binned data from DOY 128–218 (Fig. 23, top panels) and from DOY 311–035 (Fig. 23, bottom panel). Thus it becomes obvious that the scale height increases from winter to summer; a larger increase is observed during the day—from 59 to 68 km (about 15%). It is interesting that at equinox night the lowest values are not at the equatorial latitudes but at the higher latitudes near the ion trough.

5. Empirical modelling of the plasma scale height

Considering the analysis of the plasma scale height variations, it becomes quite obvious that an

empirical model would be very helpful for many purposes.

A new empirical model is currently being developed. In this model, the plasma scale height is approximated by a multi-variable polynomial delivering the scale height values with respect to season, LT, and geomagnetic latitude:

$$P(C,N;X) = \sum_{I} C(I)G(I,X) = \sum_{i_1=1}^{n_1}\sum_{i_2=1}^{n_2}\sum_{i_3=1}^{n_3} C(i_1,i_2,i_3)g_1(i_1,x_1) \times g_2(i_2,x_2)g_3(i_3,x_3), \quad (3)$$

where $C(I) = C(i_1,i_2,i_3)$—coefficients, $G(I,X) = g_1(i_1,x_1)g_2(i_2,x_2)g_3(i_3,x_3)$—generalised basis function, $N = (n_1,n_2,n_3)$—number of basis functions, $I=(i_1,i_2,.i_3)$, $i_m=1,2,...,n_m$; $m=1,2,3$—indices, $X = \prod_{m=1}^{3}[x_L^{(m)}, x_R^{(m)}]$, $x \in X \subset \Re^3$—variables and the set (g_1, g_2, g_3) is a system of linearly independent functions (basis) on the domain of the mth parameter x_m. Most commonly used bases are (cf. Press et al., 1992): the algebraic basis ($\{x^k\}$, $k = 0,1,2,\ldots$), trigonometric ($\{\sin(kx), \cos(kx)\}$, $k = 0,1,2,\ldots$), Tchebishev ($\{\cos(k\arccos(x))\}$, $k = 2,3,4\ldots$), etc. The use of algebraic polynomials is the easiest way of approximating all types of the level variations securing high accuracy near the data points. The trigonometric approximation is very useful when approximating a periodic function; the set is orthogonal over any interval and the derivative of each member is also a member. The Tchebishev polynomials are orthogonal in the interval $[-1,1]$ over a weight $(1-x^2)^{-1/2}$, and the approximation using these polynomials provides the smallest maximum deviation from the 'true' function. The method of least-squares fit is applied for determining the coefficients.

Using the analysis presented in the previous parts and based on the median observations, a preliminary version of the described model has been developed and exemplary calculations are presented here (Fig. 24). In this version, algebraic bases only have been used: 2nd degree polynomial for the seasonal variations, 4th degree polynomial for the LT variations, and 3rd degree polynomial for the latitudinal variations. The initial model evaluation shows standard deviations of 4.48 (−0.06 skewness) for the winter and 3.66 (−0.562 skewness) for the summer approximation.

The model is regularly being upgraded in step with the growing IRO measurement database. When sufficient observations become available, solar activity dependence will be also included. So far, insufficient evidence has been accumulated as to the longitudinal behaviour and the effects of ionospheric/magnetic storms on the topside scale height, in order to be able to add the storm-time changes into the model.

6. Summary and conclusion

Presented were results from the analysis of the topside plasma scale height based on recent IRO measurements carried out onboard the CHAMP satellite. At this stage, the following conclusions can be made.

The study has provided further confirmation of the sensitivity of the ionospheric scale height to the ionosphere–plasmasphere temperature, composition and dynamics. However, the dependence also proved to be much more complicated than previously thought.

After removing the storm-time values, the scale height shows a rather weak dependence on solar

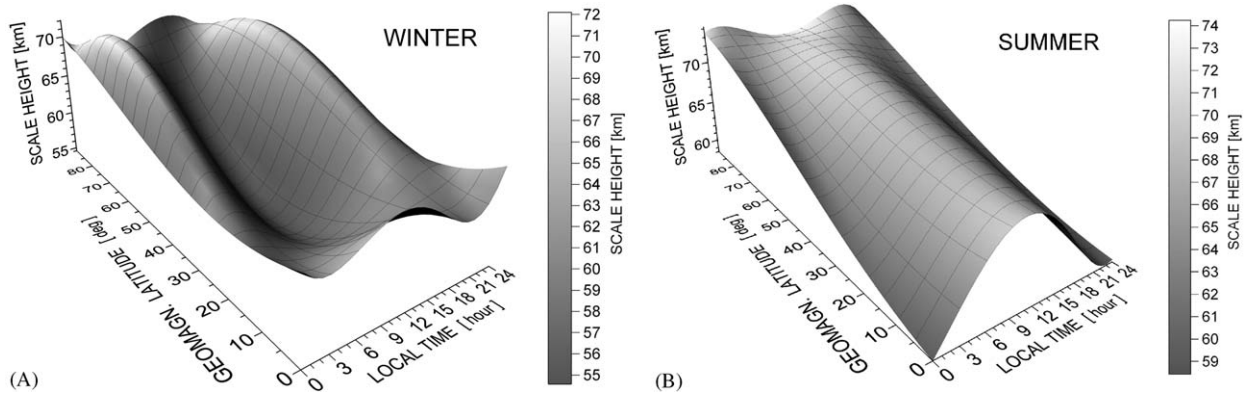

Fig. 24. CHAMP IRO topside plasma scale height: empirical modelling of diurnal-latitudinal variations for winter and summer seasons.

activity, except during winter. Particularly interesting are the following two cases: the winter daytime minimum observed between F10.7 = 120 and 150 at middle latitudes, and the steady decrease at higher solar activity during winter night-time at high latitudes.

Although the magnetic activity seems to not significantly influence the H_{sc} behaviour at low latitudes, it enhances the H_{sc} values at higher latitudes during both day- and night-time.

It is clear that the scale height generally increases in poleward directions, particularly during equinox and summer.

Strong seasonal differences are observed at middle latitudes where daytime median values in summer are about 50% higher than in winter.

Diurnal variations appear to be very complex—in some cases the daytime values are higher and in others—the night-time values; additionally, differences are detected from season to season and from latitude to latitude. All this requires additional observations from independent sources to be employed. The link between the scale height and the slab thickness has been confirmed and seems to be quite strong. In particular, the pre-dawn and post-sunset enhancements seem to be a regular and common feature for middle latitudes. Further correlative studies would definitely boost the knowledge of both the scale height and the slab thickness.

No significant longitudinal and hemispheric differences have been detected so far.

It has been shown that it is possible to utilise the IRO observations onboard CHAMP for acquiring a valuable knowledge of the plasma scale height behaviour, which in turn can be successfully applied in the development and improvement of electron density reconstruction techniques, development and validation of both empirical and theoretical models, and ionosphere composition studies.

Based on the presented analysis, a first version of a new empirical model is being developed, which will be capable of delivering the scale height with respect to latitude, local time, and season. Model results can be directly implemented into the density profile retrieval procedure by delivering an improved initial guess. In view of this direct implementation, we presented our results for the topside ionospheric scale height as deduced from formula (2) instead of presenting the real topside plasma scale height values (see the comments in Section 2.4).

It should be noted also that, due to limitations in the database and the influence of the PIM model on the determination of H_{sc}, we expect that the absolute values of H_{sc} will probably experience some corrections. Possible sources of error are the use constant scale height and Chapman ionosphere model during the profile reconstruction procedure. Nevertheless, we claim that the climatology of the H_{sc} variations is well captured and that the approach of using IRO measurements is feasible and reliable. Validation of the presented results using independent data (e.g. topside sounding measurements) are currently under way and will be presented in a follow-on publication.

Acknowedgements

This research is funded by the German Aerospace Centre (DLR), the German State Government of Mecklenburg-Vorpommern under Grant V230-630-08-TIFA-334, and by the NATO Science Program under Grant EST.CLG.979784. Ionosonde and topside sounding data obtained from the NOAA Environmental Satellite Data and Information Service.

References

Akasofu, S.-I., Chapman, S., 1972. Solar-Terrestrial Physics. Oxford University Press, Oxford.

Bailey, G.J., Sellek, R., 1992. Field-aligned flows of H^+ and He^+ in the mid-latitude topside ionosphere at solar maximum. Planetary and Space Science 40, 751–762.

Banks, P.M., Kockarts, G., 1973. Aeronomy. Academic Press, New York and London.

Beynon, W.J.G., Williams, P.J.S., 1978. Incoherent scatter of radio waves from the ionosphere. Reports on Progress in Physics 41, 909–947.

Bilitza, D., 2001. International Reference Ionosphere 2000. Radio Science 36, 261–275.

Bowles, K.L., 1958. Observations of vertical-incidence scatter from the ionosphere at 41Mc/s. Physics Review Letters 1 (12), 454–455.

Brace, L.H., Theis, R.F., 1978. An empirical model of the interrelationship of electron temperature and density in the daytime thermosphere at solar minimum. Geophysical Research Letters 5, 275–278.

Brace, L.H., Theis, R.F., 1981. Global empirical models of ionospheric electron temperature in the upper F-region and plasmasphere based in situ measurements from the Atmosphere Explorer-C, ISIS-1 and ISIS-2 satellites. Journal of Atmospheric and Solar-Terrestrial Physics 43 (12), 1317–1343.

Buonsanto, M.J., 1999. Ionospheric storms—a review. Space Science Reviews 88, 563–601.

Buonsanto, M.J., Foster, J.C., Sipler, D., 1992. Observations from Millstone Hill during the geomagnetic disturbances of

March and April 1990. Journal of Geophysical Research 97, 1225–1243.

Davies, K., 1990. Ionospheric Radio. Peter Peregrinus Ltd., London.

Davies, K., 1996. Ionosphere models. In: Dieminger, W., Hartmann, G.K., Leitinger, R. (Eds.), The Upper Atmosphere—Data Analysis and Interpretation. Springer, Berlin, pp. 693–705.

Davies, K., Liu, X.M., 1991. Ionospheric slab thickness in middle and low latitudes. Radio Science 26 (4), 997–1005.

Della-Rose, D.J., Sojka, J.J., Zhu, L., 1999. Resolving geomagnetic disturbances using K-like geomagnetic indices with variable time intervals. Journal of Atmospheric and Solar-Terrestrial Physics 61, 1179–1194.

Farley, D.T., 1996. Incoherent scatter radar probing. In: Kohl, H., Ruester, R., Schlegel, K. (Eds.), Modern Ionospheric Science. European Geophysical Society, Katlenburg-Lindau, pp. 415–439.

Foerster, M., Jakowski, N., 2000. Geomagnetic storm effects on the topside ionosphere and plasmasphere. Surveys in Geophysics 21, 47–87.

Fox, M.W., Mendillo, M., Klobuchar, J.A., 1991. Ionospheric equivalent slab thickness and its modeling applications. Radio Science 26, 429–438.

Franklin, C.A., Maclean, M.A., 1969. The design of swept-frequency topside sounders. Proceedings of IEEE 57, 897–929.

Fuller-Rowell, T.J., Codrescu, M.V., Moffett, R.J., Quegan, S., 1994. Response of the thermosphere and ionosphere to geomagnetic storms. Journal of Geophysical Research 99, 3893–3914.

Fuller-Rowell, T.J., Codrescu, M.V., Rishbeth, H., Moffett, R.J., Quegan, S., 2000. On the seasonal response of the thermosphere and ionosphere to geomagnetic storms. Journal of Geophysical Research 101 (A2), 2343–2353.

Furman, D.R., Prasad, S.S., 1973. Ionospheric slab thickness; its relation to temperature and dynamics. Journal of Geophysical Research 78, 5837.

Gordon, W.E., 1958. Incoherent scatter of radio waves by free electrons with applications to space exploration by radar. Proceedings of IRE 46, 1824.

Hanson, W.B., Ortenburger, I.B., 1961. The coupling between the protonosphere and the normal F region. Journal of Geophysical Research 66, 1425–1435.

Hanson, W.B., Patterson, T.N.L., 1964. The maintenance of the night-time F-layer. Planetary and Space Science 12, 979–997.

Hargreaves, J.K., 1992. The Solar-Terrestrial Environment. Cambridge University Press, Cambridge.

Heise, S., Jakowski, N., Wehrenpfennig, A., Reigber, C., Luehr, H., 2002. Sounding of the topside ionosphere/plasmasphere based on GPS measurements from CHAMP: initial results. Journal of Geophysical Research 29 (14).

Horwitz, J.L., Comfort, R.H., Richards, P.G., Chappell, C.R., Chandler, M.O., Anderson, P., Hanson, W.B., Brace, L.H., 1990. Plasmasphere–ionosphere coupling: 2. Ion composition measurements at plasmaspheric and ionospheric altitudes and comparison with modelling results. Journal of Geophysical Research 95, 7949–7959.

Jackson, J.E., 1969. The reduction of topside ionograms to electron density profiles. Proceedings of the IEEE 57, 960–976.

Jakowski, N., Tsybulya, K., 2004. Comparison of ionospheric radio occultation CHAMP data with IRI 2001. Advances in Radio Science 2, 275–279.

Jakowski, N., Bettac, H.D., Lazo, B., Lois, L., 1981. Seasonal variations of the columnar electron content of the ionosphere observed in Havana from July 1974 to April 1975. Journal of Atmospheric and Terrestrial Physics 43 (1), 7–11.

Jakowski, N., Schlueter, S., Sardon, E., 1999. Total electron content of the ionosphere during the geomagnetic storm on 10 January 1997. Journal of Atmospheric and Solar-Terrestrial Physics 61, 299–307.

Jakowski, N., Heise, S., Wehrenpfennig, A., Schlueter, S., Reimer, R., 2002a. GPS/GLONASS-based TEC measurements as a contributor for space weather forecast. Journal of Atmospheric and Solar-Terrestrial Physics 64 (5–6), 729–735.

Jakowski, N., Wehrenpfennig, A., Heise, S., Reigber, C., Luehr, H., Grunwaldt, L., Meehan, T., 2002b. GPS radio occultation measurements of the ionosphere from CHAMP: early results. Journal of Geophysical Research 29 (10).

Jakowski, N., Heise, S., Wehrenpfennig, A., Tsybulya, K., 2004. Ionospheric radio occultation measurements and space weather. In: Kirchengast, G., Foelsche, U., Steiner, A. (Eds.), Occultations for Probing Atmosphere and Climate. Springer, Berlin, pp. 441–446.

Jakowski, N., Tsybulya, K., Stankov, S.M., Wehrenpfennig, A., 2005a. About the potential of GPS radio occultation measurements for exploring the ionosphere. In: Reigber, Ch., Luehr, H., Schwintzer, P., Wickert, J. (Eds.), Earth Observation with CHAMP—Results from Three Years in Orbit. Springer, Berlin, pp. 441–446.

Jakowski, N., Tsybulya, K., Mielich, J., Belehaki, A., Altadill, D., Jodogne, J.C., Zolesi, B., 2005b. Validation of GPS ionospheric radio occultation results onboard CHAMP by vertical sounding observations in Europe. In: Reigber, Ch., Luehr, H., Schwintzer, P., Wickert, J. (Eds.), Earth Observation with CHAMP—Results from Three Years in Orbit. Springer, Berlin, pp. 447–452.

Jodogne, J.C., Stankov, S.M., 2002. Ionosphere–plasmasphere response to geomagnetic storms studied with the RMI-Dourbes comprehensive database. Annals of Geophysics 45 (5), 629–647.

Kutiev, I., Muhtarov, P., 2001. Modeling of midlatitude F region response to geomagnetic activity. Journal of Geophysical Research 106 (A8), 15501–15509.

Kutiev, I., Stankov, S.M., 1994. Relative abundance of H^+ and He^+ in the outer ionosphere. Advances in Space Research 14 (12), 139–141.

Kutiev, I., Stankov, S.M., Marinov, P., 1994. Analytical expression of O^+–H^+ transition surface for use in IRI. Advances in Space Research 14 (12), 135–138.

Matsushita, S., 1967. Geomagnetic disturbances and storms. In: Matsushita, S., Campbell, W.H. (Eds.), Physics of the Geomagnetic Phenomena. Academic Press, New York, pp. 1153–1202.

Mayaud, P.N., 1980. Derivation, Meaning, and Use of Geomagnetic Indices. Geophysical Monograph Series (22). AGU, Washington, DC.

Mendillo, M., Buonsanto, M.J., Klobuchar, J.A., 1975. The construction and use of storm-time corrections for ionospheric F-region parameters. In: Goodman, J.M. (Ed.), Effects of the Ionosphere on Space Systems and

Communications. Naval Research Laboratory, Washington, DC, pp. 361–371.

Menvielle, M., Berthelier, A., 1991. The K-derived planetary indices: description and availability. Reviews of Geophysics 29 (3), 415–432.

Mikhailov, A.V., Foster, J.C., 1997. Daytime thermosphere above Millstone Hill during severe geomagnetic storms. Journal of Geophysical Research 102, 17275–17282.

Mikhailov, A.V., Schlegel, K., 1998. Physical mechanism of strong negative effects in the daytime ionospheric F2-region observed with EISCAT. Annales Geophysicae 16, 602–608.

Moffett, R.J., Bailey, G.J., Jenkins, B., 1992. Effects of greatly increased O^+ loss in the ionospheric F-region. Planetary and Space Science 40, 1631–1637.

O'Loughlin, K., 1997. SPIDR on the Web: Space Physics Interactive Data Resource on-line analysis tool. Radio Science 32 (5), 2021–2026.

Oyama, K.-I., Balan, N., Watanabe, S., Takahashi, T., Isoda, F., Bailey, G.J., Oya, H., 1996. Morning overshoot of Te enhanced by downward plasma drift in the equatorial topside ionosphere. Journal of Geomagnetism and Geoelectricity 48, 959–966.

Oyama, K.-I., Abdu, M.A., Balan, N., Bailey, G.J., Watanabe, S., Takahashi, T., Paula, E.R., Batista, I.S., Isoda, F., Oya, H., 1997. High electron temperature associated with the prereversal enhancement. Journal of Geophysical Research 102, 417–424.

Parkinson, W.D., Hutton, V.R.S., 1989. The electrical conductivity of the Earth. In: Jacobs, J.A. (Ed.), Geomagnetism, vol. 3. Academic Press, London, pp. 261–322.

Pavlov, A.V., Abe, T., Oyama, K.-I., 2000. Comparison of the measured and modelled electron density and temperatures in the ionosphere and plasmasphere during 20–30 January 1993. Annales Geophysicae 18, 1257–1272.

Pfaff, R.F., 1996. In-situ measurement techniques for ionospheric research. In: Kohl, H., Ruester, R., Schlegel, K. (Eds.), Modern Ionospheric Science. European Geophysical Society, Katlenburg-Lindau, pp. 459–551.

Press, W.H., Flannery, B.P., Teukolsky, S.A., Vetterling, W.T., 1992. Numerical Recipes in C. Cambridge University Press, New York.

Proelss, G.W., 1995. Ionospheric F-layer storms. In: Volland, H. (Ed.), Handbook of Atmospheric Electrodynamics, vol. 2. CRC Press, Boca Raton, pp. 195–248.

Rastogi, R.G., 1988. Collapse of the equatorial ionosphere during the sunrise period. Annales Geophysicae 6, 205.

Rawer, K., 1988. Synthesis of ionospheric electron density profiles with Epstein functions. Advances in Space Research 8 (4), 191–198.

Rawer, K., 1993. Wave Propagation in the Ionosphere. Kluwer Academic Publishers, The Netherlands.

Reigber, C., Luehr, H., Schwintzer, P. (Eds.), 2003. First CHAMP Mission Results for Gravity, Magnetic and Atmospheric Studies. Springer, Berlin.

Reinisch, B.W., 1996. Ionosonde. In: Dieminger, W., Hartmann, G.K., Leitinger, R. (Eds.), The Upper Atmosphere—Data Analysis and Interpretation. Springer, Berlin, pp. 370–381.

Reinisch, B.W., Huang, X., 2001. Deducing topside profiles and total electron content from bottomside ionograms. Advances in Space Research 27 (1), 23–30.

Spalla, P., Jakowski, N., Wehrenpfennig, A., Spencer, P.S., Mitchell, C.N., 2003. Verification of CHAMP radio occultation observations in the ionosphere using MIDAS. In: Reigber, Ch., Luehr, H., Schwintzer, P. (Eds.), First CHAMP Science Mission Results for Gravity, Magnetic and Atmospheric Studies. Springer, Berlin, pp. 545–550.

Stankov, S.M., 1990. A new coordinate change in mathematical modelling of the upper ionosphere. Comptes Rendus de l'Academie Bulgare des Sciences 43 (11), 29–31.

Stankov, S.M., 1996a. A steady-state F-region model and its use for satellite data analysis. Annali di Geofisica 39 (5), 905–924.

Stankov, S.M., 1996b. Modelling the light-ion densities in the ionosphere. Annali di Geofisica 39 (6), 1149–1156.

Stankov, S.M., 2002a. Empirical modelling of ion transition levels based on satellite in-situ measurements. Comptes Rendus de l'Academie Bulgare des Sciences 55 (1), 35–40.

Stankov, S.M., 2002b. Evaluation of theoretical profilers used in the electron density profile reconstruction. Acta Geodaetica et Geophysica Hungarica 37 (4), 385–401.

Stankov, S.M., Jakowski, N., 2005. Topside plasma scale height modeling based on CHAMP measurements: first results. In: Reigber, C., Luehr, H., Schwintzer, P., Wickert, J. (Eds.), Earth Observations with CHAMP—Results from Three Years in Orbit. Springer, Berlin, pp. 459–464.

Stankov, S.M., Jakowski, N., Heise, S., Muhtarov, P., Kutiev, I., Warnant, R., 2003a. A new method for reconstruction of the vertical electron density distribution in the upper ionosphere and plasmasphere. Journal of Geophysical Research 108 (A5), 1164.

Stankov, S.M., Warnant, R., Jodogne, J.C., 2003b. Real-time reconstruction of the vertical electron density distribution from GPS-TEC measurements. Acta Geodaetica et Geophysica Hungarica 38 (4), 377–388.

Stankov, S.M., Jakowski, N., Heise, S., 2005. Reconstruction of ion and electron density profiles from space-based measurements of the upper electron content. Planetary and Space Science 53 (9), 945–957.

Stolle, C., Jakowski, N., Schlegel, K., Rietveld, M., 2004. Comparison of high latitude electron density profiles obtained with the GPS radio occultation technique and EISCAT measurements. Annales Geophysicae 22 (6), 2015–2022.

Su, Y.Z., Bailey, G.J., Balan, N., 1994. Night-time enhancements in TEC at equatorial anomaly latitudes. Journal of Atmospheric and Terrestrial Physics 56, 1619–1628.

Su, Y.Z., Oyama, K.-I., Bailey, G.J., Takahashi, T., Oya, H., 1996. Longitudinal variations of the topside ionosphere at low latitudes: satellite and mathematical modelings. Journal of Geophysical Research 101, 17191–17205.

Szuszczewicz, E.P., Lester, M., Wilkinson, P., Blanchard, P., Abdu, M., Hanbaba, R., Igarashi, K., Pulinets, S., Reddy, B.M., 1998. A comparative study of global ionospheric responses to intense magnetic storm conditions. Journal of Geophysical Research 103 (A6), 11665–11684.

Taylor Jr., H.A., 1971. Evidence of solar geomagnetic seasonal control of the topside ionosphere. Planetary and Space Science 19, 77–93.

Titheridge, J.E., 1973. The slab thickness of the mid-latitude ionosphere. Planetary and Space Science 21, 1775–1793.

Van Zandt, T.E., 1967. The neutral atmosphere and the quiet ionosphere. In: Matsushita, S., Campbell, W.H. (Eds.), Physics of the Geomagnetic Phenomena. Academic Press, New York, p. 509.

Van Zandt, T.E., Bowles, K.K., 1960. Use of the incoherent scatter technique to obtain ionospheric temperatures. Journal of Geophysical Research 65, 2627.

Van Zandt, T.E., Clark, W.L., Warnock, J.M., 1972. Magnetic apex coordinates: a magnetic coordinate system for the ionospheric F2 layer. Journal of Geophysical Research 77 (A13), 2406–2411.

Wehrenpfennig, A., Jakowski, N., Wickert, J., 2001. A dynamically configurable system for operational processing of space weather data. Physics and Chemistry of the Earth (C) 26 (8), 601–604.